Lawrence Berkeley Laboratory

UNIVERSITY OF CALIFORNIA

Physics Division

To be published in the Proceedings of the 1984 DPF Summer Study on the Design and Utilization of the Superconducting Super Collider, Snowmass, CO, June 23 - July 13, 1984

SEARCHING FOR SUPERSYMMETRY AT THE SSC

S. Dawson, A. Savoy-Navarro, G. Alverson, R.M. Barnett, E. Fernandez, J. Freeman, L. Gladney, H. Haber, S. Lynn, F. Paige, and R. Wagner

October 1984

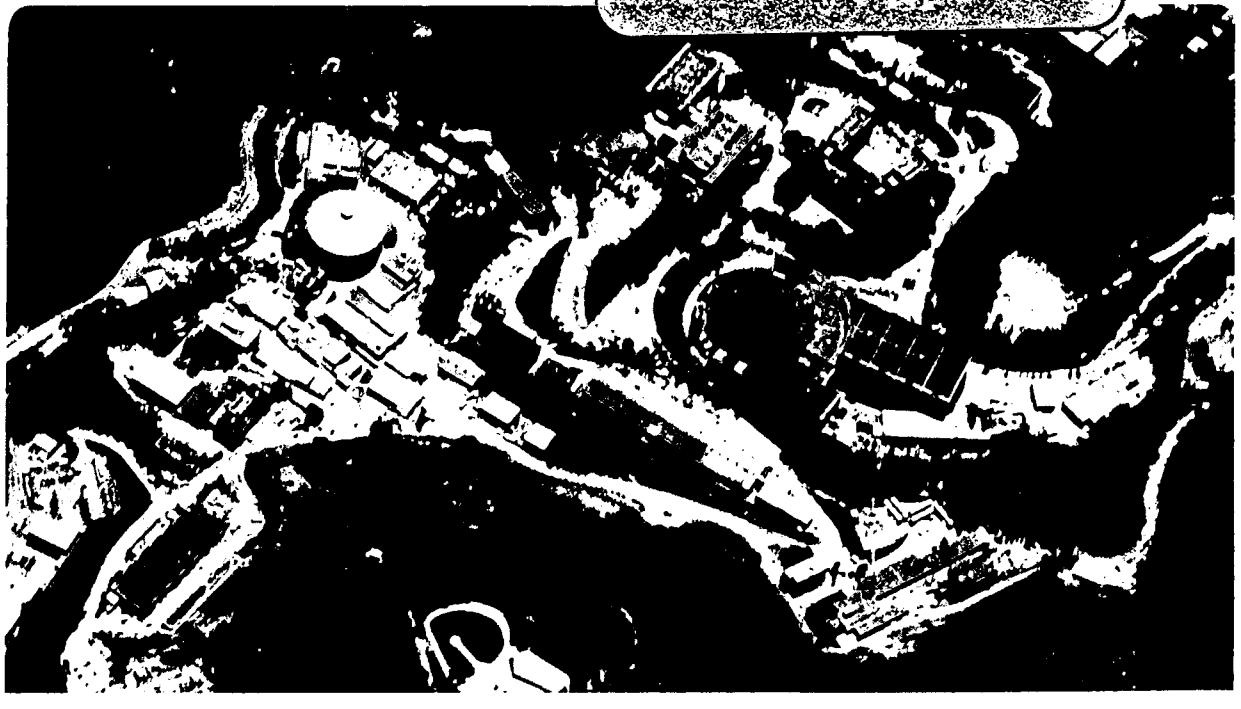

Prepared for the U.S. Department of Energy under Contract DE-AC03-76SF00098

DISCLAIMER

October 1984 LBL-18479

SEARCHING FOR SUPERSYMMETRY AT THE SSC

A contribution to the
Proceedings of the 1984 DPF Summer Study
on the Design and Utilization of the
Superconducting Super Collider
June 23 - July 13, 1984
Snowmass, Colorado 81611

Sally Dawson

Lawrence Berkeley Laboratory
University of California
Berkeley, California 94720

and

Aurore Savoy-Navarro

CEA - Saclay
Gif-sur-Yvette, France

G. Alverson, *Northeastern Univ.*
R.M. Barnett, *LBL*
E. Fernandez, *Univ. of Colorado*
J. Freeman, *Fermilab*
L. Gladney, *SLAC*
H. Haber, *Univ. of California, Santa Cruz*
S. Lynn, *SUNY, Stony Brook*
F. Paige, *BNL*
R. Wagner, *ANL*

This work was supported by the Director, Office of Energy Research, Office of High Energy and Nuclear Physics, Division of High Energy Physics of the U.S. Department of Energy under Contract DE-AC03-76SF00098.

Summary

A detailed study of the prospects for finding the new particles predicted by supersymmetric theories at the SSC is made. A study of the signatures, background, and detector requirements necessary to find these particles is presented.

I. Introduction

Supersymmetric (SUSY) models have generated increasing amounts of attention in recent years as a means of under standing the roles of scalar particles in a field theory. Since supersymmetry connects fermions and bosons in a natural framework, theorists are hopeful that it will reduce the freedom surrounding fermions and scalars in the Weinberg-Salam model. No satisfactory model exists at this time, but the structure of the supersymmetric algebra is sufficiently attractive to warrant a serious study of its consequences.[1,2,3,4,5] It is possible to make a great many predictions which are independent of the choice of a specific model. In this report we make a detailed attempt to study the experimental problems posed by super symmetric theories and to analyze the capabilities of an SSC to find the many new particles predicted by these theories.

The plan of this report is as follows. In Section II, we discuss the present theoretical situation of supersymmetric phenomenology and briefly review the results contained in the literature. The experimental signatures for the production of various SUSY particles are examined in Section III with varying assumptions about the SUSY masses and decay scenarios. In Section IV, we discuss the background from known physics to events containing the new SUSY particles. We pay particular attention to the two jet background. Section V contains a discussion of the characteristics of events containing SUSY particles, including the E_t missing spectra and the average number of jets per event. We also consider here the trigger requirements necessary to identify SUSY particles. The results of two detector simulations are presented in Section VI. One is a classical 4π detector for which we have used the CDF simulation package and the other is a simple 4π calorimeter. Finally, in Section VII, we briefly discuss a Monte Carlo written by R. M. Barnett and H. Haber and compare their results with those obtained from ISAJET. We end with some conclusions in Sections VIII.

II. Theoretical Background

In this report, we consider an effective low energy N=1 supersymmetric version of the standard SU(3) x SU(2) x U(1) model of the strong and electroweak interactions. We stress that our conclusions do not depend upon the details of any specific supersymmetric model. To every known particle, there is associated a supersymmetric partner differing from the ordinary particle by 1/2 unit of spin and with all other quantum numbers identical. Among the observed particles there are no candidates for pairs related by supersymmetry, hence the spectrum is effectively doubled in SUSY theories. If the supersymmetry were exact, each particle would be degenerate in mass with its superpartner. Since this is not the case, the supersymmetry must be broken and the superpartners must acquire masses. The masses of these particles, however, depend on the details of the model and we will treat them as free parameters. The theory we analyze has two scalars associated with each of the known fermions, (one couples to the left-handed fermion and the other to the right-handed fermion), a Majorana fermion corresponding to each gauge boson and a Majorana fermion for each Higgs boson. (Supersymmetric models require at least two SU(2) Higgs doublets in order to give masses to both the charge 2/3 and the charge-1/3 quarks). The SUSY particles and their quantum numbers are listed in Table 1.

Table 1. Supersymmetric Partners of SU(3)xSU(2)xU(1) Particles

particles	spin	color	charge	R-number
g gluon	1	8	0	0
$\tilde{g}$ gluino	1/2	8	0	1
γ photon	1	0	0	0
$\tilde{\gamma}$ photino	1/2	0	0	1
$W^{\pm}$,Z intermediate bosons	1	0	±1,0	0
$\tilde{W}^{\pm}$,$\tilde{Z}$ wino,zino	1/2	0	±1,0	1
q quark	1/2	3	2/3,-1/3	0
$\tilde{q}$ squark	0	3	2/3,-1/3	$-\chi=\pm1$
e electron	1/2	0	-1	0
$\tilde{e}$ selectron	0	0	-1	$-\chi=\pm1$
ν neutrino	1/2	0	0	0
$\tilde{\nu}$ sneutrino	0	0	0	1
H^{+},H^{0} Higgs	0	0	1,0	0
H'^{0},H'^{-} Higgs	0	0	0,-1	0
$\tilde{H}^{+}$,$\tilde{H}^{0}$ Higgsino	1/2	0	1,0	1
$\tilde{H}'^{0}$,$\tilde{H}'^{-}$ Higgsino	1/2	0	0,-1	1

At this point it is useful to introduce some terminology. All of the SUSY particles are denoted by a tilde over the symbol for the known particle with which they are associated. The scalar partner of a fermion is called a sfermion and the fermionic partner of a gauge boson or a Higgs boson is a gaugino or Higgsino, respectively. For example, the scalar partner of a quark is written as $\tilde{q}$ and called a squark, while the fermionic partner of the photon is the photino, $\tilde{\gamma}$.

In many SUSY theorys, there is a conserved quantum number associated with the supersymme try - the "R number". This quantum number is 0 for the conventional particles and ± 1 for the SUSY particles(see Table 1). Experimentally, a conserved R invariance means that SUSY particles are always produced in pairs. The R symmetry is, however, broken by the Majorana mass terms which give the gauginos mass. In the class of models which we examine there remains a residual of the R symmetry which ensures that SUSY particles are always pair produced. Models without this symmetry have been considered by many authors.[6]

SUSY particles have been searched for in e^+e^- annihilations, in hadronic beam dump experiments and by examining cosmological constraints and some limits have been placed on their masses. The current limits on SUSY particles are summarized in Refs. 4 and 5. By the time of the SSC quite stringent limits will exist on the masses of SUSY particles, (or else SUSY will have been discovered!). The Fermilab Tevatron will see gluinos or squarks if they are lighter lighter than 130 GeV, photinos lighter than 160 GeV, and winos and zinos with masses less than 100 GeV. In addition SLC and LEP will be able to see selectrons up to masses near 50 GeV. We will thus concentrate on finding SUSY particles with masses in the 100 GeV to 1 TeV range.

One of the beauties of supersymmetric theories is that the interactions of SUSY particles with matter are completely specified, leaving only the masses and some mixing angles as free parameters. This means that all cross sections can be calculated unambiguously in terms of these quantities. The complete expressions for the pair production of all SUSY particles are given in Refs. [4] and [7]. The cross sections for producing all possible combinations of two SUSY particles have been calculated by Eichten et al.,[3] (EHLQ), for SSC energies with cuts on the rapidities of the produced particles. In all of their plots they have assumed that the produced SUSY particles have equal masses. In Figs. 1-3, we show $\sigma(pp \to \tilde{g}\tilde{\gamma})$, $\sigma(pp \to \tilde{g}\tilde{q})$, and $\sigma(pp \to \tilde{g}\tilde{W}^+ + \tilde{g}\tilde{W}^-)$ for unequal SUSY masses corresponding to those which we will analyze in detail later. The structure functions we use are those of EHLQ with $\Lambda_{QCD} = .29$ GeV. In Fig. 2, we have summed over all flavors of squarks (which we assumed to have degenerate masses).

It is also useful to have angular distributions for the production of SUSY particles. In Figs. 4-7, we plot $E\,d\sigma/dp^3$ versus p_t for the inclusive production of gluinos, photinos, winos, and squarks, respectively, at 90°'s in the center of mass. We have chosen representative masses for the SUSY particles in order to illustrate various scenarios which are possible. In Figs. 4-6, we have kept separate the contributions to the differential cross section from the case where both of the final state particles are gauginos and the case where one particle is a gaugino and the other is a squark. For light gluino masses, ($m_{\tilde{g}} \lesssim 1$ TeV), the dominant contribution to the gluino production cross section is from $pp \to \tilde{g}\tilde{g}$, while for heavier gluinos (and $m_{\tilde{q}} = m_{\tilde{g}}$), the major contribution is from $pp \to \tilde{g}\tilde{q}$. For the sets of SUSY masses we have considered, the dominant

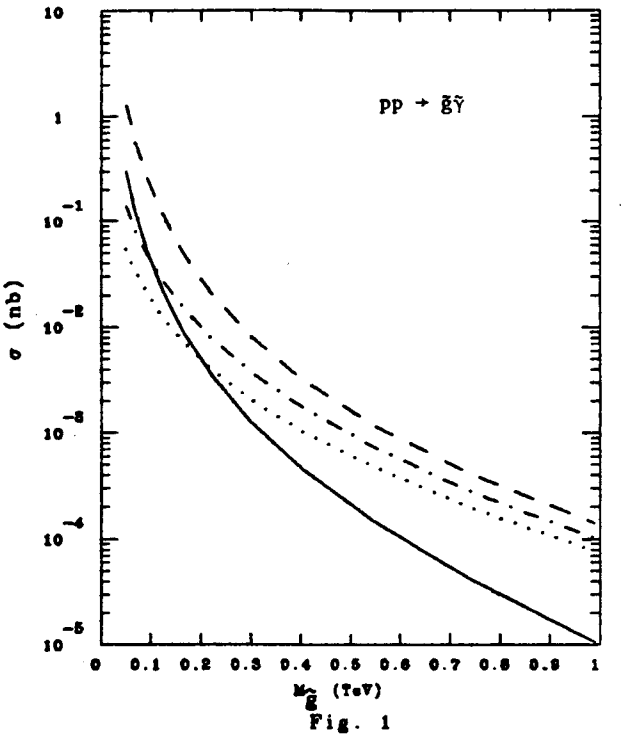

Fig. 1

Fig. 1. $\sigma(pp \to \tilde{g}\tilde{\gamma})$ at $\sqrt{s} = 40$ TeV. The solid, dashed, dot-dashed, and dotted curves have $m_{photino} = m_{gluino}$ and $m_{photino} = 1$, 100, and 200 GeV, respectively. All curves have $m_{squark} = m_{gluino}$.

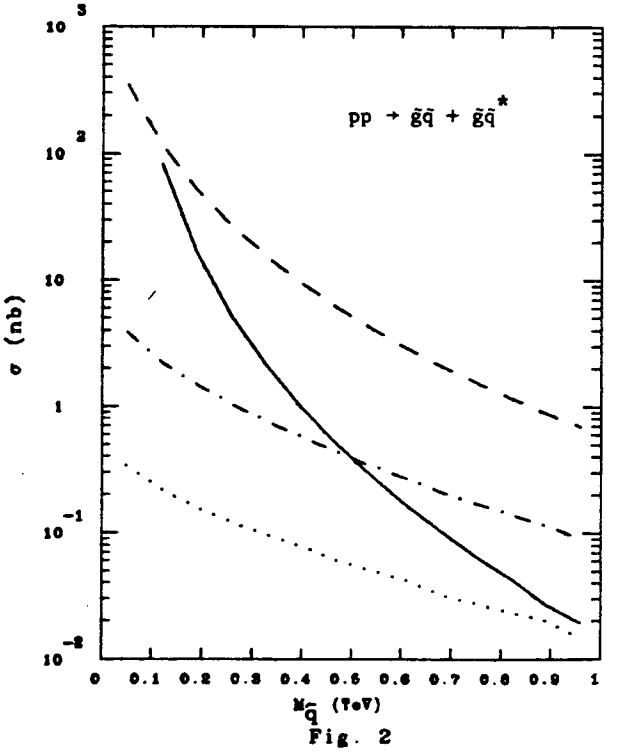

Fig. 2

Fig.2. $\sigma(pp \to \tilde{g}\tilde{q}+\tilde{g}\tilde{q}^*)$ at $\sqrt{s}$=40 TeV. The solid, dashed, dot-dashed, and dotted curves have $m_{squark}=m_{gluino}$ and m_{gluino}=100, 500, and 1000 GeV, respectively. We have summed over squark flavors.

contribution to inclusive $\tilde{W}$ (or $\tilde{\gamma}$) production is from $pp \to \tilde{W}\tilde{q}$ (or $pp \to \tilde{\gamma}\tilde{q}$). Similarly, in Fig. 7 the contributions from $pp \to \tilde{q}$ + gaugino and $pp \to \tilde{q}\tilde{q}^*$ are shown separately. In Figs. 4-7, we have summed over squark flavors.

EHLQ calculate the production of wino, $\tilde{W}$, and zino, $\tilde{Z}$, gauge eigenstates by neglecting any possible mixing of the gauginos with the Higgsinos. The $\tilde{W}^+$ can mix with the $\tilde{H}^+$, the $\tilde{W}^-$ can mix with $\tilde{H}'^-$, and the $\tilde{Z}$ can mix with the $\tilde{\gamma}$, $\tilde{H}'^0$ and $\tilde{H}^0$, to form the mass eigenstates. The details of this mixing depend upon the model and are discussed in Ref. [4], [5] and [8]. The model dependence due to such mixing effects affects the two-body cross sections for all SUSY particles with the exception of gluino pair production. (In any specific model, of course, the masses and mixing angles are completely specified.)

An example of such mixing occurs in the production of two charged gauginos, (these are the mass eigenstate mixture of a wino and a Higgsino). The complete expression for this cross section is given in Appendix B of Ref. [4] and in Ref. [8] and depends upon two model dependent mixing angles, ϕ_+ and ϕ_-, and the eigenvalues of the mass matrix, (which may be either positive or negative). The mass eigenstates are:

$$\tilde{\omega}_1^+ = -i\cos\phi_+\tilde{W}^+ + \sin\phi_+\tilde{H}^+$$

$$\tilde{\omega}_1^- = -i\cos\phi_-\tilde{W}^- + \sin\phi_-\tilde{H}'^-$$

$$\tilde{\omega}_2^+ = i\sin\phi_+\tilde{W}^+ + \cos\phi_+\tilde{H}^+$$

$$\tilde{\omega}_2^- = i\sin\phi_-\tilde{W}^- + \cos\phi_-\tilde{H}'^-$$

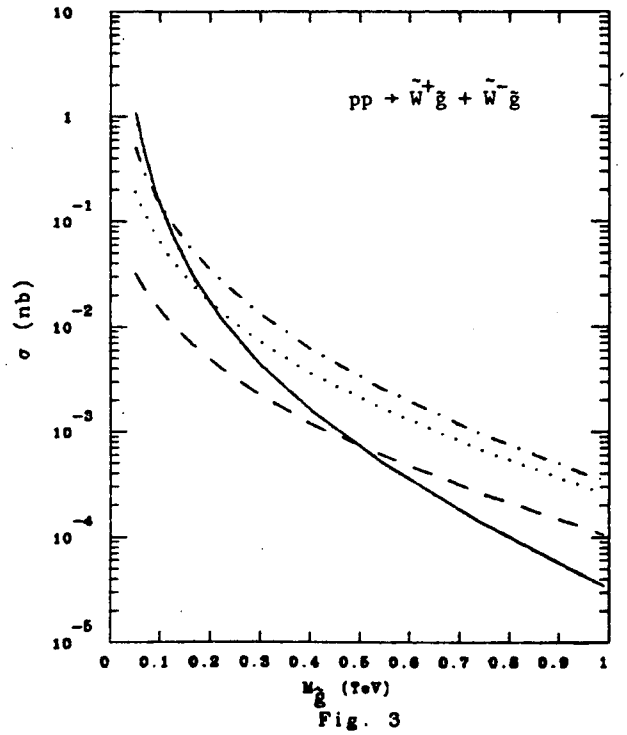

Fig. 3

Fig 3. $\sigma(pp \to \tilde{W}^+\tilde{g} + \tilde{W}^-\tilde{g})$ at $\sqrt{s}$ = 40 TeV. The solid, dashed, dot-dashed, and dotted curves have $m_{wino} = m_{gluino}$ and m_{wino} = 500 , 100, and 200 GeV, respectively. All curves have $m_{gluino} = m_{squark}$.

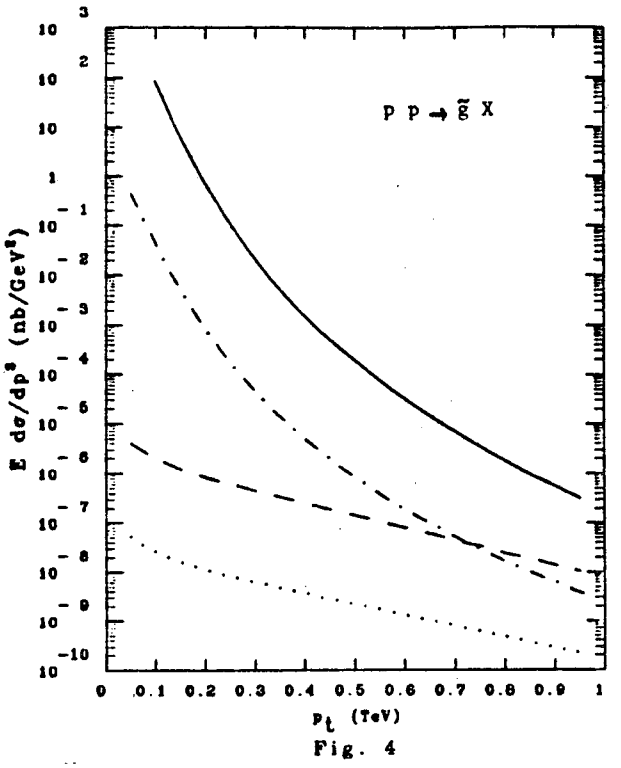

Fig. 4

Fig. 4. $E\,d\sigma/dp^3$ for $pp \to \tilde{g}X$ at $\sqrt{s}$ = 40 TeV. The solid and dashed curves have m_{gluino} = 100 GeV and 1 TeV, respectively, and include only the contributions from $pp \to \tilde{g}$ + ($\tilde{\gamma}$, $\tilde{Z}$, $\tilde{W}$, or $\tilde{g}$). The dot-dashed and dotted curves have m_{gluino} = 100 GeV and 1 TeV, respectively, and include only the contribution from $pp \to \tilde{g}$ + squark. All gauginos and squarks have equal masses.

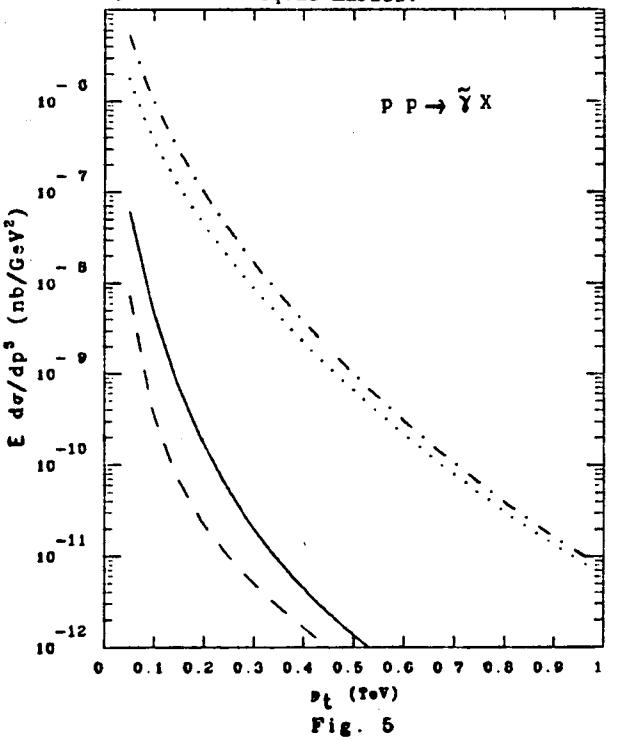

Fig. 5

Fig. 5. $E\,d\sigma/dp^3$ for $pp \to \tilde{\gamma}X$ at $\sqrt{s}$ = 40 TeV. The solid and dashed curves have $m_{photino} = 0$, m_{gluino} = 100 GeV and 500 GeV, and m_{squark} = 500 and 600 GeV, respectively, and include only the contributions from $pp \to \tilde{\gamma}$ + ($\tilde{\gamma}$, $\tilde{Z}$, $\tilde{W}$, or $\tilde{g}$). The dot-dashed and dotted curves have $m_{photino} = 0$, m_{gluino} = 100 and 500 GeV, and m_{squark} = 500 GeV and 600 GeV, respectively, and include only the contribution of $pp \to \tilde{\gamma}$ + squark. All curves have $m_{\tilde{W}} = m_{\tilde{Z}} = m_{\tilde{g}}$.

Figure 8 illustrates the effects of varying the mixing angles and the signs of the mass eigenstates on the values of the cross section. For light gauginos these effects are small at SSC energies, but as the gaugino mass nears 1 TeV they become significant.

In general, there are a variety of decay channels open to each of the SUSY particles. In many models, one (or more) of the SUSY particles will be stable or there will be stable bound states of two or more SUSY particles. We will not comment on this possibility except to emphasize the importance of stable particle searches in finding the new physics associated with supersymmetry. The spectrum of stable bound states has been discussed in Ref. [5]. We consider the following decay scenarios for the gluino;

1. Stable $\tilde{g}$,

2. $\tilde{g} \to q\bar{q}\tilde{\gamma}$ with $\tau = 48\,\pi\, m_{\tilde{q}}^4/(\alpha\alpha_s e_q^2 m_{\tilde{g}}^5)$

where e_q is the quark charge and $m_{\tilde{q}}$ and $m_{\tilde{g}}$ are the squark and gluino masses. The signal for the gluino decays will be 1 or 2 jets and missing energy from the $\tilde{\gamma}$ which escapes the detector unseen. This will be discussed in detail in Section III. The possible existence of a light Goldstino $\tilde{G}$, (the Goldstone boson of spontaneously broken super symmetry), has been ignored by us. In models with a Goldstino it is possible to have the decay $\tilde{g} \to g\tilde{G}$.

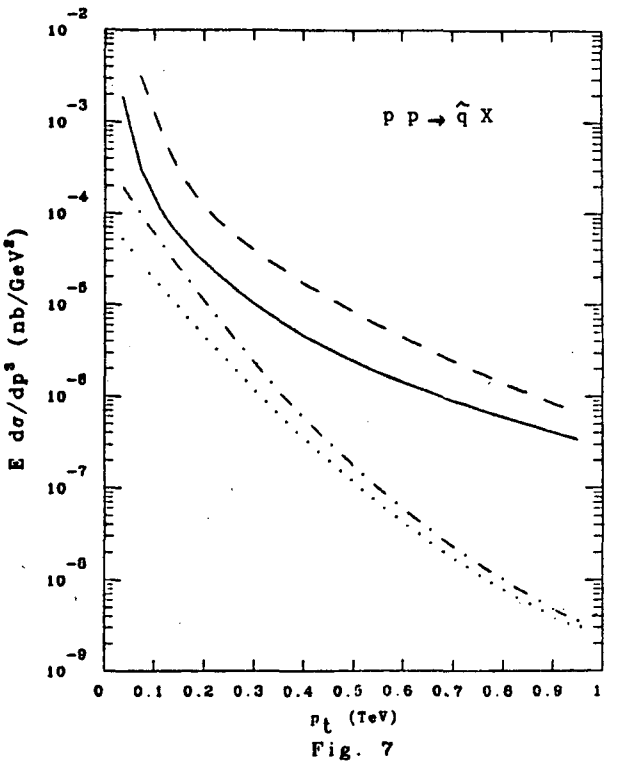

Fig. 7

Fig. 7. E dσ/dp³ for pp → $\tilde{q}$ + X. The solid and dashed lines have m_{gluino} = 200 and 500 GeV, m_{squark} = 500 and 200 GeV, and $m_{photino}$ = 0, respectively, and include only the contributions of pp → $\tilde{q}\bar{q}^*$. The dotted and dot-dashed curves have m_{squark} = 200 and 500 GeV, m_{squark} = 500 and 200 GeV, and $m_{photino}$ = 0, respectively, and include the contributions of pp → $\tilde{q}$ + ($\tilde{\gamma}$, $\tilde{Z}$, $\tilde{W}^{\pm}$, $\tilde{g}$) and pp → $\tilde{q}^*$ + ($\tilde{\gamma}$, $\tilde{Z}$, $\tilde{W}^{\pm}$, $\tilde{g}$). m_{wino}=m_{zino}=200 GeV for all curves.

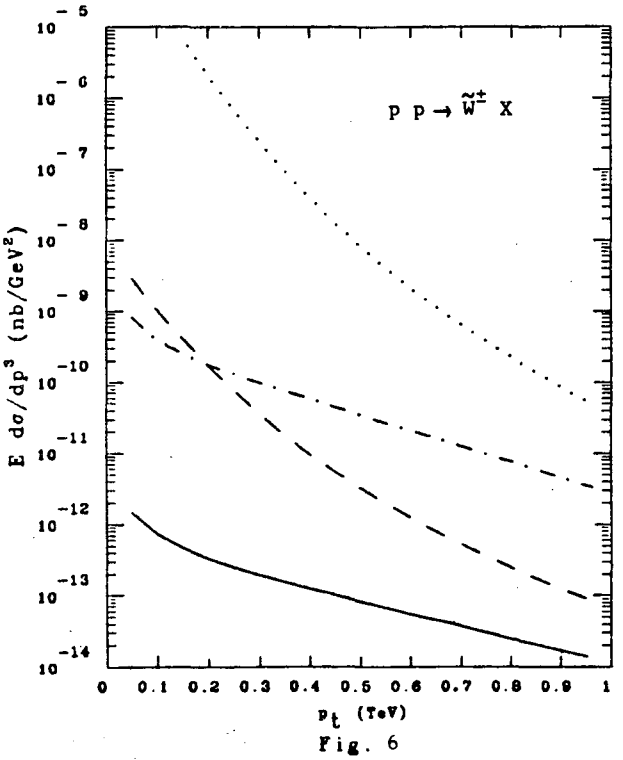

Fig. 6

Fig. 6. E dσ/dp³ for pp → $\tilde{W}^{\pm}$ + X. The solid and dashed lines have m_{wino} = 1 TeV and 200 GeV, respectively, and include only the contributions for pp → $\tilde{W}^{\pm}$ + ($\tilde{\gamma}$, $\tilde{Z}$, $\tilde{W}^{\pm}$, $\tilde{g}$). The dot-dashed and dotted lines have m_{wino} = 1 TeV and 200 GeV, respectively, and include only the contribution of pp → $\tilde{W}^{\pm}$ + squark. All gaugino and squark masses are equal.

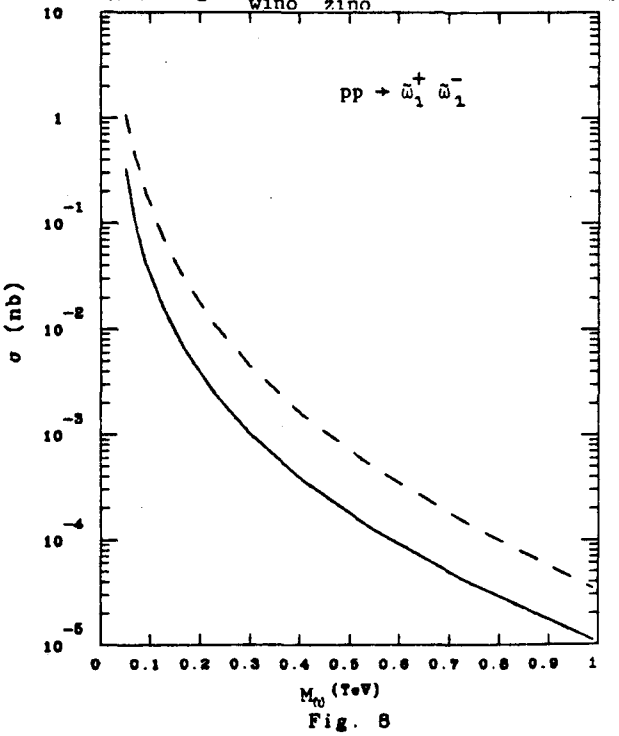

Fig. 8

Fig. 8. $\sigma(pp \to \omega_1^+ \omega_1^-)$ at $\sqrt{s}$ = 40 TeV, where ω_1 is the mass eigenstate mixture of the wino and Higgsinos. The solid line has $\cos\phi_{\pm} = 1$ and the dashed line has $\cos\phi_{\pm} = -1$. We have taken $m_{\tilde{q}} = m_{\tilde{W}}$.

The squarks can decay in several ways,

1. Stable $\tilde{q}$,

2. $\tilde{q} \to q\tilde{g}$ with $\tau = 3m_{\tilde{q}}^3/[2\alpha_s (m_{\tilde{q}}^2 - m_{\tilde{g}}^2)^2]$

3. $\tilde{q} \to q\tilde{\gamma}$ with $\tau = 2\, m_{\tilde{q}}^3/[\alpha e_q^2 (m_{\tilde{q}}^2 - m_{\tilde{\gamma}}^2)^2]$.

The squark decays 2 and 3 both lead to hadronic jets plus missing energy. We consider only the case where the photino is stable and the lightest SUSY particle, although in many models it is possible to have $\tilde{\gamma} \to \gamma\tilde{\nu}$ or $\tilde{\gamma} \to \gamma\tilde{G}$.

Wino and zino decays are potentially a rich source of information about the theory and have received much attention in the literature.[7] We consider in detail only the decay,

1. $\tilde{W} \to e\tilde{\nu}$ with $\tau = 4 \sin^2\theta_W\, m_{\tilde{W}}^3/[\alpha(m_{\tilde{W}}^2 - m_{\tilde{\nu}}^2)^2]$.

We do not consider at all the effects of supersymmetry on the decays of the W and Z bosons as the SppS and the Tevatron will have studied this question in detail long before the SSC.

We turn now to a detailed discussion of the signatures and decay sequences of the SUSY particles.

III. Experimental Signatures of SUSY Events

Our main goal during this summer study has been to go one step further compared to previous workshops[1,2]. Namely, not to remain at the phase of writing a catalogue of all the different possibilities that SUSY offers but to bring this theory to the experimental level; this means to study *realistically* how the apparatus can detect some specific SUSY processes, trigger on them, and overcome both the different backgrounds and the pile-up events which are becoming a serious problem as the beam energy of pp colliders is going up.

IIIa. SUSY Processes Considered in this Work

An attractive feature of SUSY theories is that they offer a set of reactions which taken together give a complete and self-consistent scenario. Among the possible alternatives which can be of interest for hadron-hadron colliders, we have chosen to look in detail at the following reactions:

(1.) $pp \to \tilde{g}\tilde{g}$ It should give the highest cross section for a SUSY process.

(2.) $pp \to \tilde{g}\tilde{q}$ It also has a high cross section and a rather complicated, but characteristic jet structure.

(3.) $pp \to \tilde{g}\tilde{\gamma}$ It has a lower cross section than processes (1) and (2), but a rather clean signature.

(4.) $pp \to \tilde{W}\tilde{g}$, $\tilde{W} \to \ell\nu\tilde{\gamma}$ It has a striking leptonic signal.

The reactions (1.) and (2.) have high cross sections, a multijet structure and a large amount of missing energy. Reactions (3.) and (4.) have lower cross sections, but more specific signatures.

A "free parameter" in SUSY is the mass of sparticles. So we have considered different scenarios varying the masses of the sparticles from 100 GeV to 1 TeV. Of course, if the mass spectra is more towards 100 GeV, SUSY should be already proved by the time of the SSC (unless physicists or apparatus or both are too bad!). As has already been explained in Section I, depending on the mass of the sparticles, we will have also different types of decays. Taking into account these two different "degrees of freedom" we have imagined for our study the set of scenarios described in Table 2.

We now describe the tools we have used to do this job.

Table 2

Set of SUSY scenarios considered in our study

SUSY process	Decay mode for involved SUSY particle	Mass range
$pp \to \tilde{g}\tilde{g}$	$\tilde{g} \to q\bar{q}\tilde{\gamma}$	$m_{\tilde{g}} = 100$ GeV $m_{\tilde{q}} = 100$ GeV
$pp \to \tilde{g}\tilde{g}$	$\tilde{g} \to q\bar{q}\tilde{\gamma}$	$m_{\tilde{g}} = 1$ TeV $m_{\tilde{q}} = 1$ TeV
$pp \to \tilde{g}\tilde{q}$	$\tilde{g} \to q\bar{q}\tilde{\gamma}$ $\tilde{q} \to q\tilde{g}$	$m_{\tilde{g}} = 200$ GeV $m_{\tilde{q}} = 500$ GeV
$pp \to \tilde{g}\tilde{q}$	$\tilde{g} \to q\bar{q}\tilde{\gamma}$ $\tilde{q} \to q\tilde{\gamma}$	$m_{\tilde{g}} = 500$ GeV $m_{\tilde{q}} = 200$ GeV
$pp \to \tilde{g}\tilde{\gamma}$	$\tilde{g} \to q\bar{q}\tilde{\gamma}$ $\tilde{\gamma}$ stable	$m_{\tilde{g}} = 100$ GeV $m_{\tilde{\gamma}} \simeq 0$
$pp \to \tilde{g}\tilde{\gamma}$	$\tilde{g} \to q\bar{q}\tilde{\gamma}$ $\tilde{\gamma}$ stable	$m_{\tilde{g}} = 500$ GeV $m_{\tilde{\gamma}} \simeq 0$
$pp \to \tilde{W}\tilde{g}$	$\tilde{W} \to \ell\tilde{\nu}$, $\tilde{\nu} \to \nu\tilde{\gamma}$ $\tilde{g} \to q\bar{q}\tilde{\gamma}$	$m_{\tilde{W}} = 200$ GeV $m_{\tilde{g}} = 200$ GeV $m_{\tilde{\gamma}} = 0$ GeV
$pp \to \tilde{W}\tilde{g}$	$\tilde{W} \to \ell\tilde{\nu}$, $\tilde{\nu} \to \nu\tilde{\gamma}$ $\tilde{g} \to q\bar{q}\tilde{\gamma}$	$m_{\tilde{W}} = 1$ TeV $m_{\tilde{g}} = 1$ TeV $m_{\tilde{\gamma}} = 0$ GeV

IIIb. Description of the Tools Used in this Work

We need a Monte Carlo to generate events, a simulation package to study the effects of different detectors, and a jet finder to describe the jet structure of each event.

Among the different generators available on the market, we have chosen to use ISAJET.[9] This choice has been motivated by the following considerations:

1. It is a multipurpose Monte Carlo in the sense that it has been written to generate most of the usual pp or $p\bar{p}$ reactions such as the production of light constituents and heavy quarks, the Drell-Yan process, W and Z production (with both leptonic and hadronic decays), heavy lepton production, and some SUSY processes such as $\tilde{g}$ pair

production and $\tilde{g}\tilde{q}$ production. We have implemented the $\tilde{g}\tilde{\gamma}$ process and $\tilde{W}\tilde{g}$ process including the corresponding matrix elements as calculated in Ref. 4.

2. It has been adapted to the simulation of different apparatus such as the UA experiments at CERN, the CDF detector at the Fermilab Tevatron, and it is easily adaptable to other simulations. (This will be described in more detail in Section V.)

So, within its own biases and limitations, ISAJET allows us to study certain processes and their corresponding backgrounds. *)

A simple simulation has been used for the studies reported in Sections III, IV, and V. Namely, we use a calorimeter of ± 5 in pseudorapidity (η) with a granularity in (η, ϕ), (ϕ = azimuthal angle), defined by cells of 0.1 in pseudorapidity and 5°'s in azimuth which produces a rather rough granularity. The particle is put into one cell and the energy is smeared in only one cell according to a Gaussian distribution parameterized by $.15/\sqrt{E} + 0.01$ in the electromagnetic part and $0.35/\sqrt{E} + 0.01$ in the hadronic part. This sample calorimeter thus has typical uranium calorimeter characteristics.

A simple minded, but very efficient jet finder has been used for all of the jet studies reported in this paper, (apart from some of the results of Section V wich use the CDF jet finder package). This jet finder picks the highest E_t cell and then sums all cells which are within 1 unit of pseudorapidity, and have $\Delta r = \sqrt{|\Delta y|^2 + |\Delta \eta|^2} \leq 1$ and also have an E_t^{ceil} greater than 2 GeV; the other cells are thrown away. The jets reconstructed in this way but which have an E_t less than or equal to 30 GeV are also discarded.

We now have all the tools which we need to define the experimental signatures of SUSY events.

IIIc. Typical Pictures of SUSY Events

By experimental signatures we want to emphasize how well, already at the first-level trigger, SUSY-type events can be selected. The most popular way to trigger highly segmented calorimeter information is by using, at the level of a hardware processor, the "Lego plot"*) technique (see the pioneering work of the CDF experiment)[10]; so our goal in this section is to give the main characteristics of the Lego plot of the different processes we are concerned with and to picture them in this way. The results are shown in Figs. 9-12. In the two first classes of events [corresponding to reactions (1) Fig. 9 and (2) Fig. 10] and which are multiple jet events we see that we do not always get, as we could naïvely suppose, the number of q jets which corresponds to the way sparticles decay; but in fact it can vary and be 2, 3, 4 or 5 reconstructed jets. Also, we already notice that in the decay process $\tilde{g} \rightarrow q\bar{q}\tilde{\gamma}$, one of the two q jets will, in general, be a much lower p_T jet than the other one (this will be confirmed using another generator, see Section VII). The signature of $\tilde{g}\tilde{\gamma}$ appears as a very clean signature in terms of 1 or 2 jets and a large imbalance in energy (Fig. 11). The events corresponding to a $\tilde{W}\tilde{g}$ process, where the $\tilde{W}$ decays into $\ell\tilde{\nu}$ ($\tilde{\nu} \rightarrow \nu\tilde{\gamma}$), shows a very high E_T lepton, a large imbalance in energy, and clear jet structure (Fig. 12).

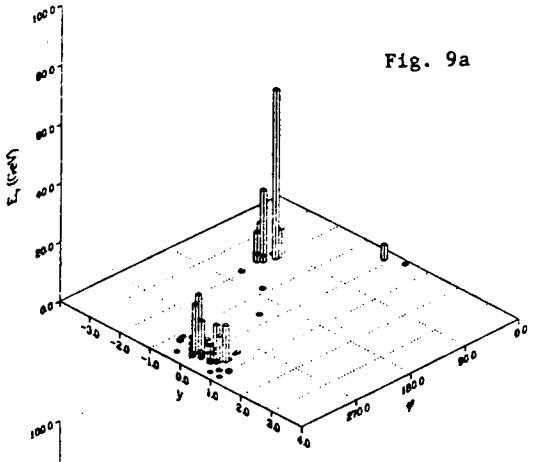
Fig. 9a

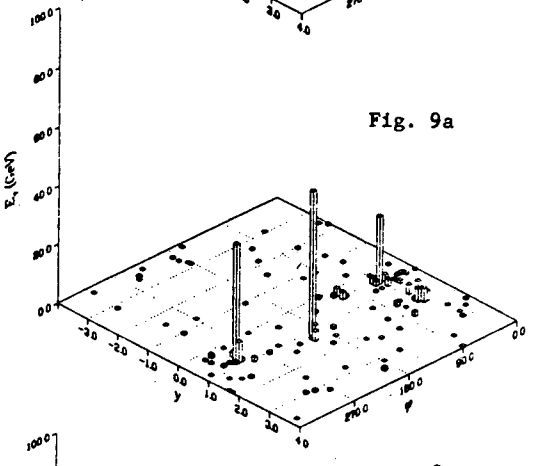
Fig. 9a

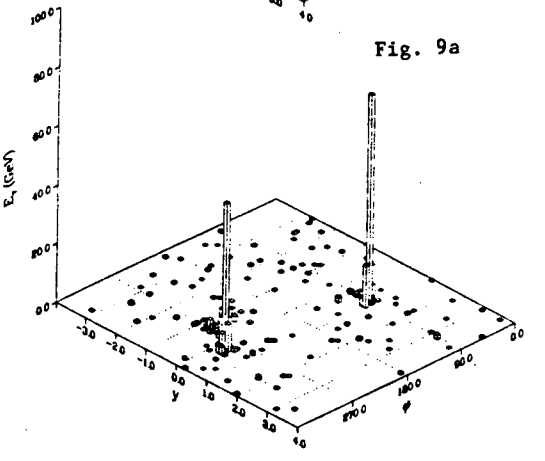
Fig. 9a

By studying the different backgrounds which can bother us in this search (Section IV), we are going to show that this first level of selection is not enough to trigger in a unique way the SUSY events. Then in Section V, we will define some more peculiar characteristics which will help to trigger on these processes.

*) Our concern in this work is not only to be as much as possible free from any theoretical prejudices, but also from the limitations of a special Monte Carlo. So we have also looked at the difference in the results obtained when using another generator (this is reported in Section VII).

*) By Lego plot we mean the (E_T, η, ϕ) three-dimensional plot of an event.

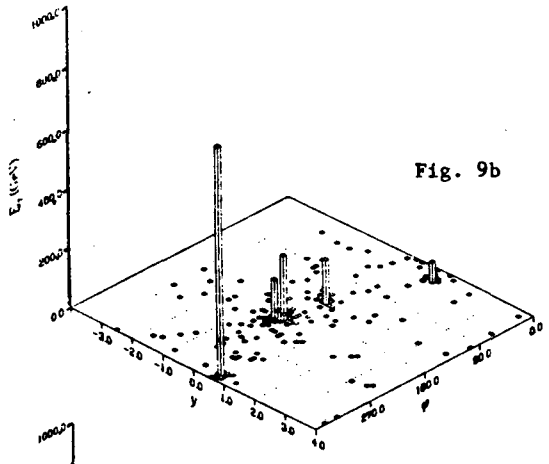

Fig. 9b

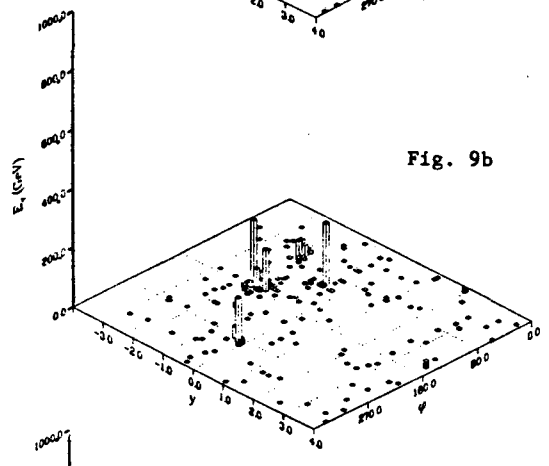

Fig. 9b

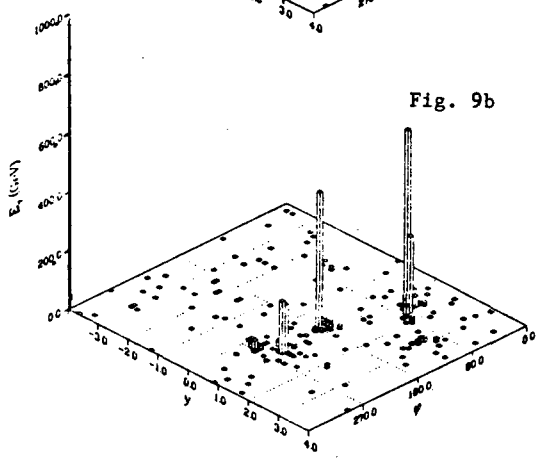

Fig. 9b

Fig. 9 Signatures of $\tilde{g}$ pair production in pp collisions: a) $m_{\tilde{g}}$ = 100 GeV; b) $m_{\tilde{g}}$ = 1 TeV.

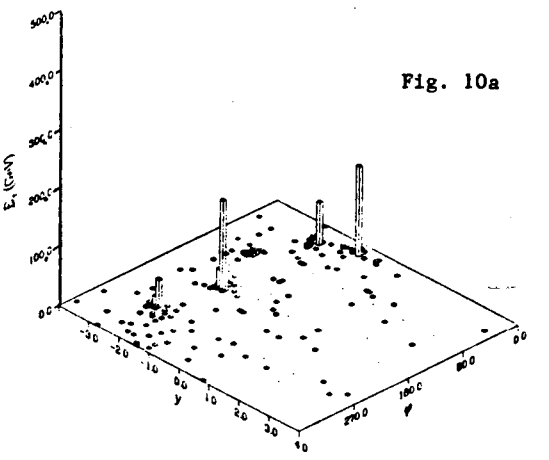

Fig. 10a

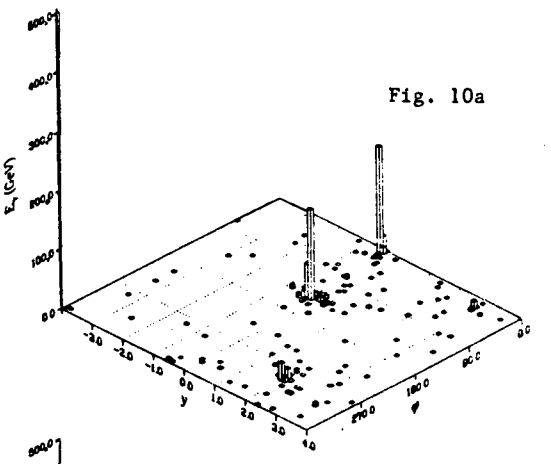

Fig. 10a

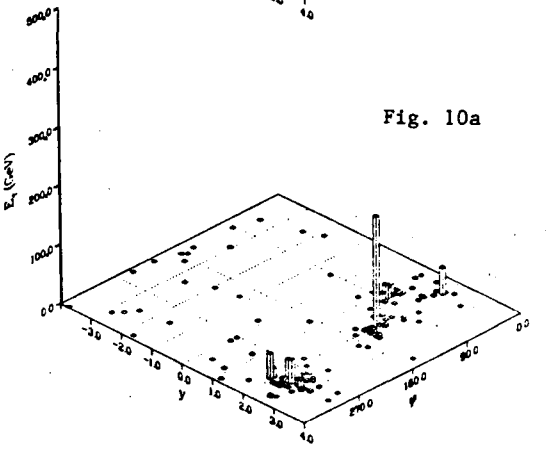

Fig. 10a

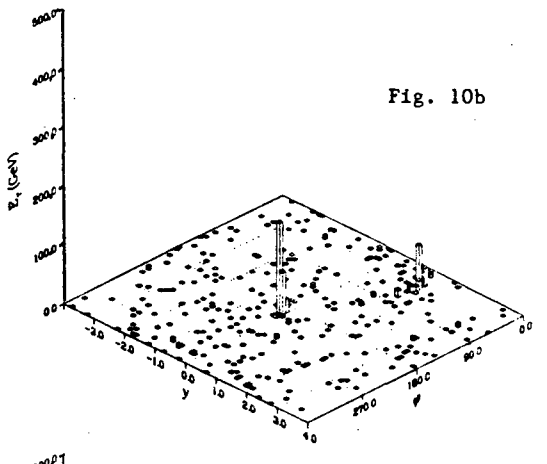

Fig. 10b

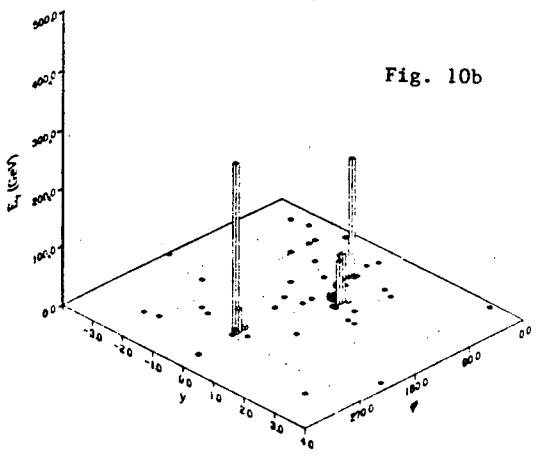

Fig. 10b

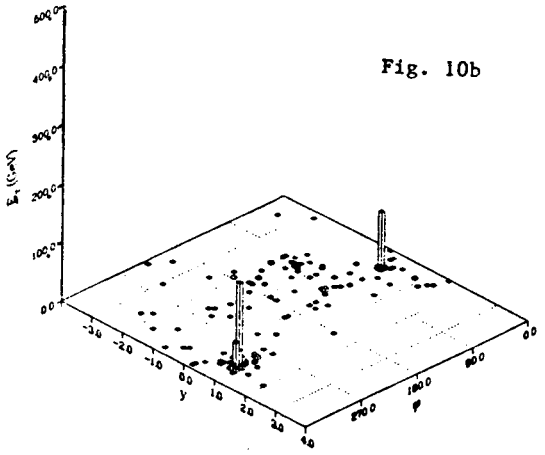

Fig. 10b

Fig. 10 Signatures of $\tilde{g}\tilde{q}$ production in pp collisions: a) $m_{\tilde{g}} = 200$ GeV, $m_{\tilde{q}} = 500$ GeV; b) $m_{\tilde{g}} = 500$ GeV, $m_{\tilde{q}} = 200$ GeV.

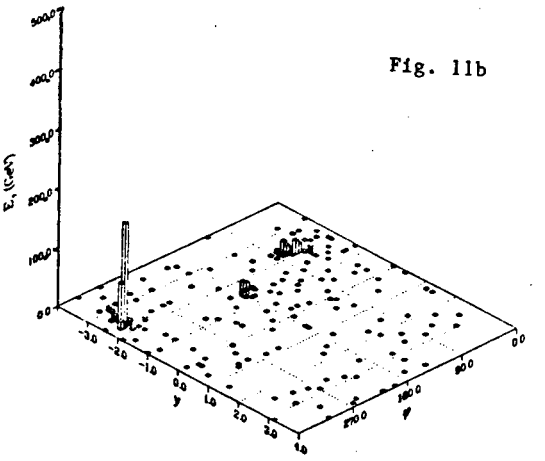

Fig. 11b

Fig. 11 Signatures of $\tilde{g}\tilde{\gamma}$ produced in pp collisions: a) $m_{\tilde{g}} = 100$ GeV, $m_{\tilde{\gamma}} = 0$ GeV; b) $m_{\tilde{g}} = 500$ GeV, $m_{\tilde{\gamma}} = 0$ GeV.

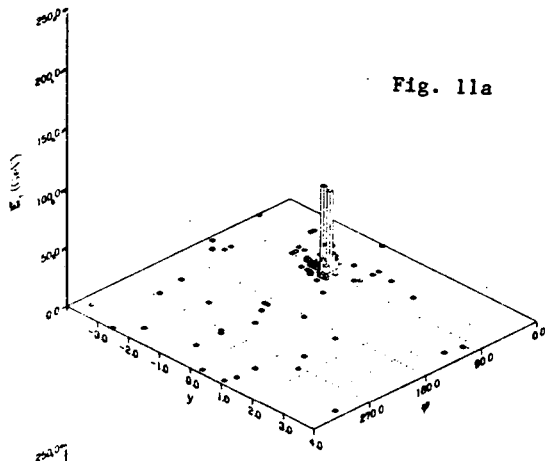

Fig. 11a

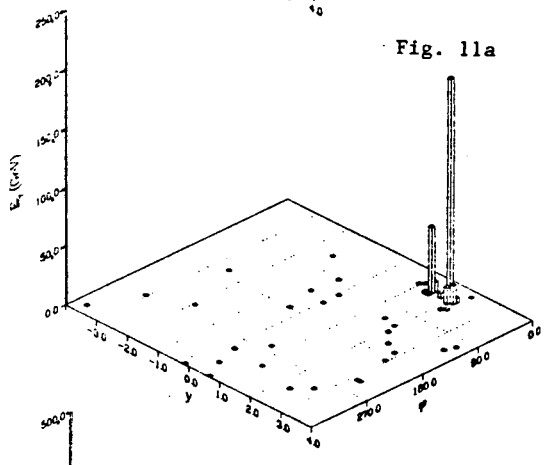

Fig. 11a

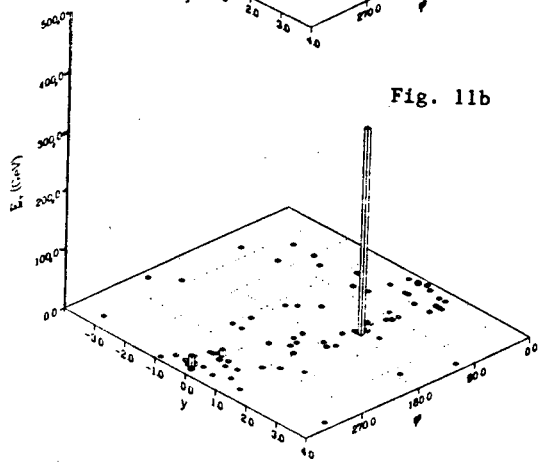

Fig. 11b

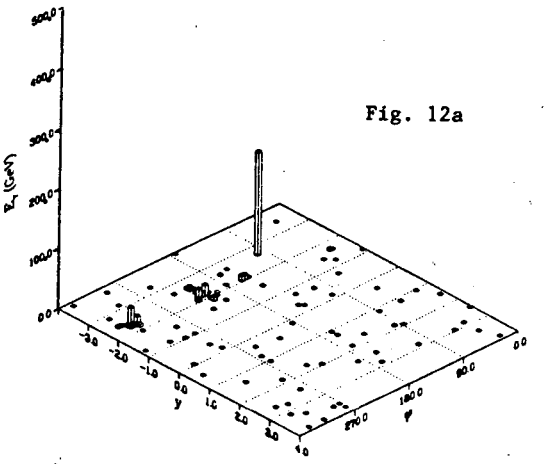

Fig. 12a

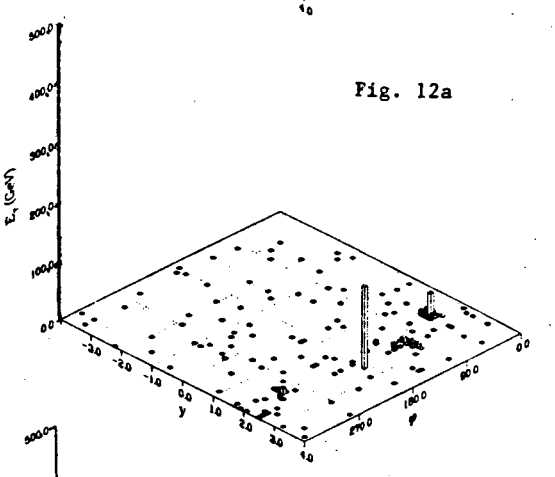

Fig. 12a

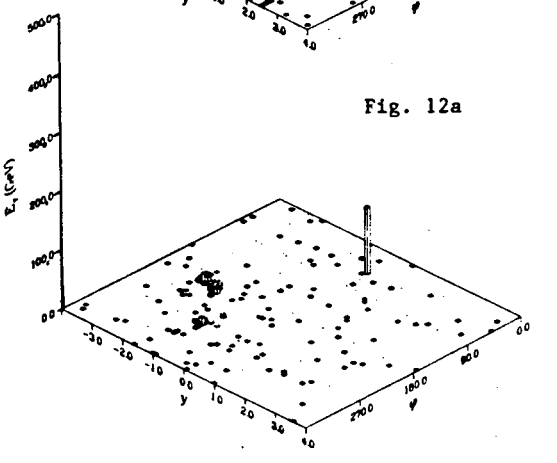

Fig. 12a

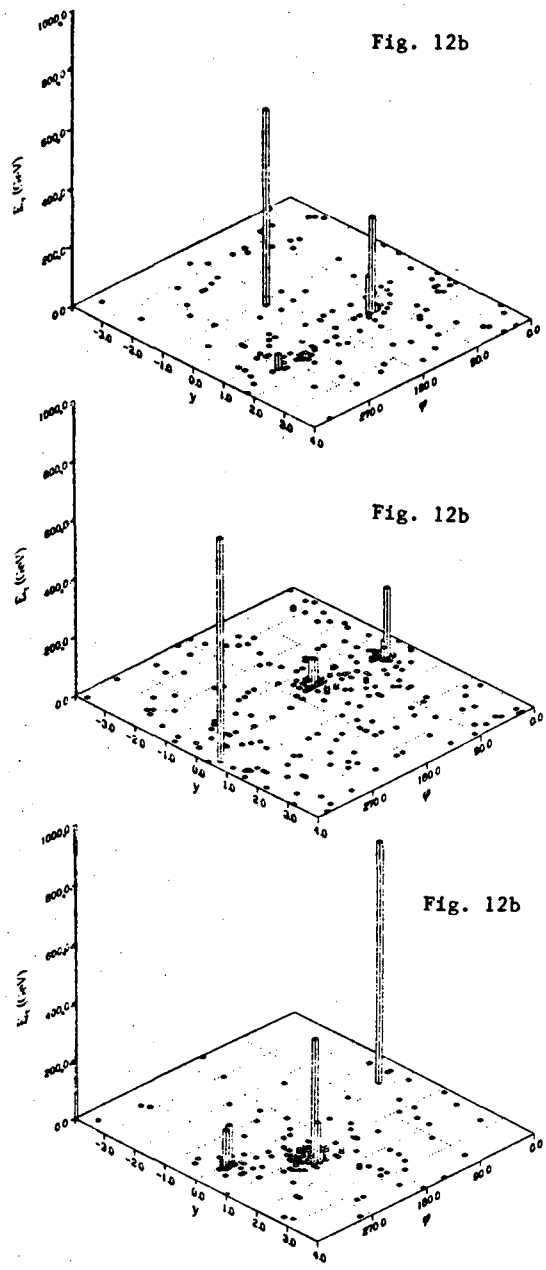

Fig. 12 Signatures of $\tilde{W}\tilde{g}$ produced in pp collisions: a) $m_{\tilde{W}} = m_{\tilde{g}} =$ 200 GeV, b) $m_{\tilde{W}} = m_{\tilde{g}} = 1$ TeV.

IV. Backgrounds and Pile Up Problems

We consider in this section the various backgrounds one has to take into account when searching for SUSY events in a pp collider; also, we pay special attention to the pile-up problem, which matters more and more as we go higher and higher in luminosity.

IVa. Standard Model Background

We have emphasized in Section III, how different SUSY processes are characterized by their jet structure, their amount of missing energy, and sometimes the presence of charged lepton(s). It has already been pointed out[1,2] that even in the case of a SUSY process which has a relatively high cross-section, such as the $\tilde{g}$ pair production, there is quite an important background due to light constituents which are abundantly produced in pp collisions. We are now going to refine the analysis of this so-called standard background. In this section we consider only gluino pair production with $m_{\tilde{g}} = 1$ TeV*).

To achieve this work, a sample of 48,000 events generated by ISAJET Monte Carlo according to the reaction pp → qq (where q = g, u, d, s, c, b, t) with jet p_T's in the range of 100 to 4000 GeV has been produced. A first selection of the interesting background is made by extracting, from these events, those which have a lepton (including charged and neutral leptons in the event) with p_T at least equal to or greater than 5%; 6,000 such events remain after applying this cut. The apparatus simulation used in this section is the same as that described in Section III.

By first looking at a Lego plot of some of these events (Fig. 13), we see how such background events can fake our search, for instance for $\tilde{g}$ pair events, if no additional cut is applied on the data other than this preliminary missing p_T cut. An estimate of the signal-to-background ratio gives, at this selection level, a value of the order of 1 to 10; the comparison between the missing energy spectra corresponding to SUSY events and the background of light constituents shows (Fig. 14) that a simple missing energy cut is not enough to handle this serious background problem. So, what we have tried to do is to use more sophisticated and appropriate cuts, namely using the x_E and x_{out} variables.

The idea in setting such variables is to measure the missing $\vec{p}_T$ relative to the highest E_T jet. It can be defined in two different ways: relative to the sphericity axis or to the axis of the highest E_T jet (the jets being defined according to our naïve jet finder already described in Section III).

i) For the sphericity analysis, we first calculate the elements of the E_T tensor as follows:

$$E_{TXX} = \Sigma_i E_{iT}^2 \cos^2 \phi_i$$

$$E_{TXY} = \Sigma_i E_{iT}^2 \cos^2 \phi_i \sin \phi_i$$

$$E_{TYY} = \Sigma_i E_{iT}^2 \sin^2 \phi_i \ ,$$

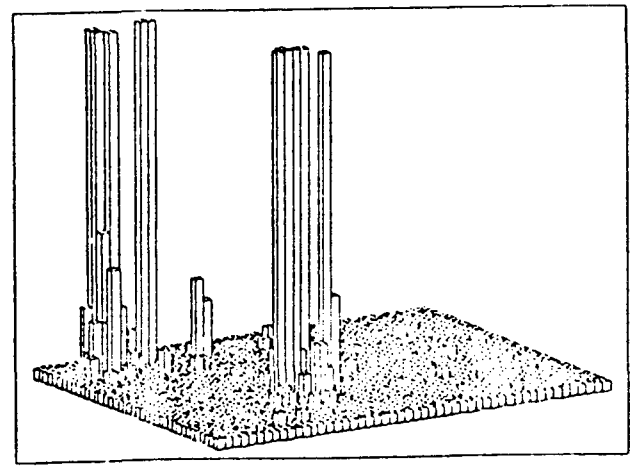

Fig. 13 QCD background: $E_j^{jet} = 1$ TeV; $E_T^{miss} = 465$ GeV.

*) We have studied the case of a high-mass gluino because the search for such a heavy object requires high luminosity.

Then we find the eigenvectors of this tensor:

$$\begin{bmatrix} E_{TXX} & E_{TXY} \\ E_{TXY} & E_{TYY} \end{bmatrix}$$

which is the sphericity tensor in the transverse plane. The components of the missing p_T are measured relative to the eigenvectors. The projection normalized to the total E_T on the major axis gives x_E, and on the minor axis gives x_{out}; in other words:

$$x_E = \vec{p}_T^{miss}/E_T^{tot}\,\hat{e}_1\,;\; x_{out} = \vec{p}_T^{miss}/E_T^{tot}\,\hat{e}_2$$

ii) For the jet basis, we take the direction of the largest jet and use it as the primary axis $\hat{e}_1$. The minor axis $\hat{e}_2$ is just $(-y, x)$ of the major axis.

In addition in this analysis all plots but the total E_T plot, are made, applying a cut of 1 TeV $< E_T^{tot} <$ 3 TeV to kill the low-E_T background while retaining most of the signal for $m_{\tilde{g}}$ = 1 TeV.

The two methods give similar results. A reasonable optimization of the x_E, x_{out} cuts has been found, if we take $x_E > 0.25$ and $x_{out} > 0.08$; the consequence is that very few background events pass this cut and we find in both cases that, after applying this selection, the gluino signal is 5.4×10^{-9} mb and the background is less than or equal to 2×10^{-10} mb. So, let us take, for instance, the sphericity version. By comparing the x_{out} distributions from events with gluino pairs (assuming $m_{\tilde{g}}$ = 1 TeV) with the one corresponding to the background containing jets with p_T (lepton)/p_T (jet) $\gtrsim$ 5%, we find (Fig. 15) that the signal dominates at x_{out} by about 0.2. It looks as if $e^{-x_{out}/0.16}$, while the background is more like to be $e^{-x_{out}/0.02}$ and to cross at x_{out} = 0.14. If we take the signal as all SUSY events above 0.2, we get 25% acceptance. The background should be down at least by an order of magnitude.

So in this case, the situation is pretty comfortable. Now let us take into consideration the effect of pile-up. Let us first explain how we have tried to simulate the pile-up in our analysis.

Fig. 14a

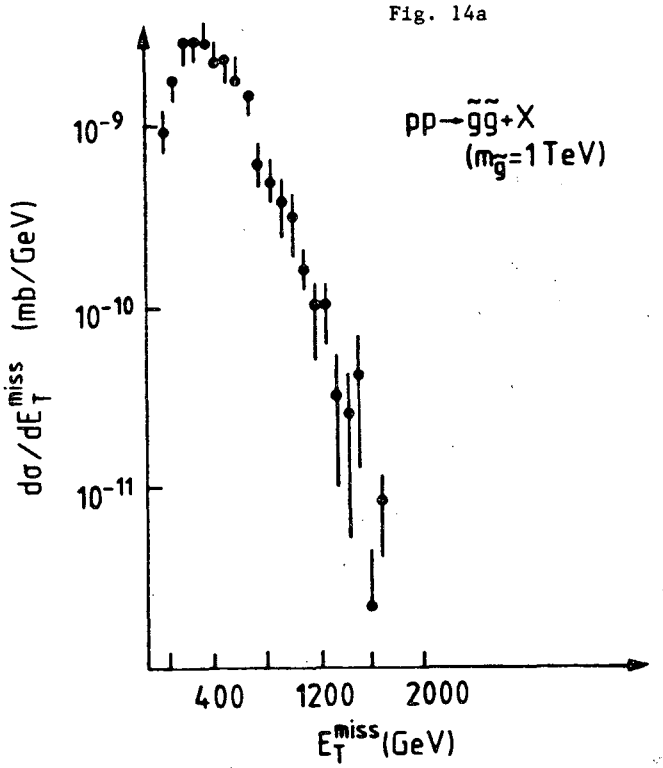

Fig. 14b

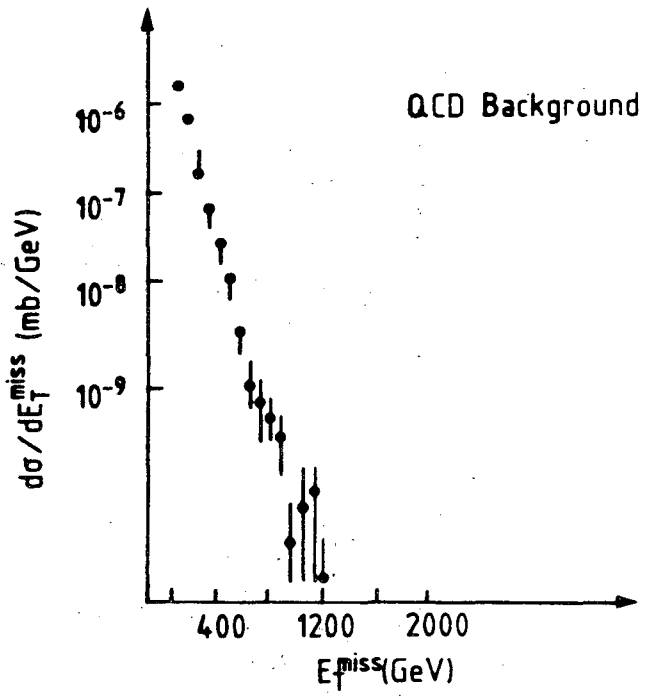

Fig. 14 Missing energy spectra a) for $pp \to \tilde{g}\tilde{g} + X$, $m_{\tilde{g}}$ = 1 TeV; b) for QCD-background.

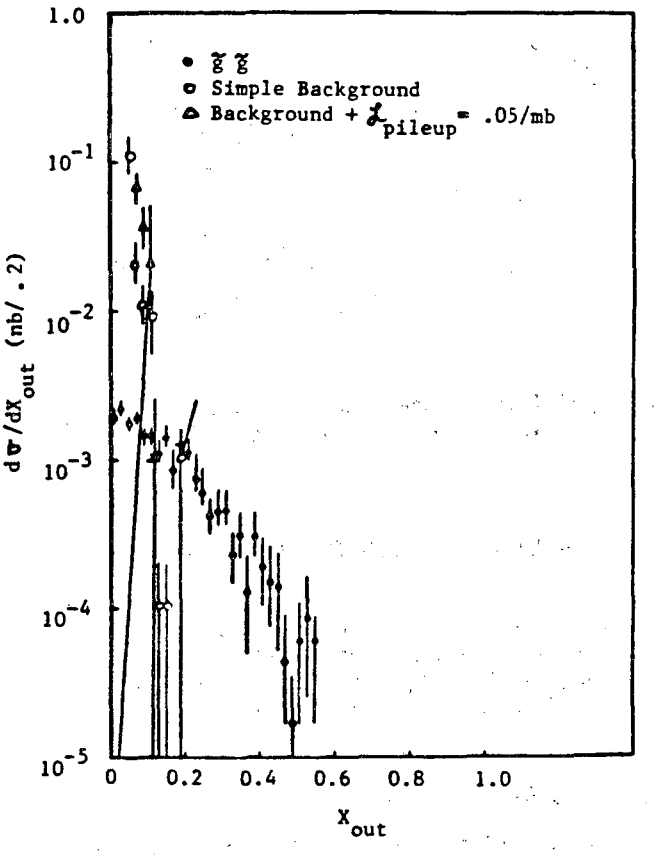

Fig. 15 X_{out} distribution.

IVb. Pile Up Problem

It has been emphasized by the QCD group[11] that the jet cross-section can be calculated using QCD perturbation theory even at very low p_T, for which $p_T/\sqrt{s}$ is much less than one. Thus a large fraction of the total cross-section contains jets with $p_T \sim 10$ GeV. To incorporate this fact we have used ISAJET to generate as our minimum bias sample a set of QCD jet events with $p_T \geq 3$ GeV; the integrated cross-section for this sample is 220 mb, in reasonable agreement with the existing fits[12] of total cross-section; at the low end of this p_T range the jets are barely visible, the events are dominated by the beam jets and so are described by an extrapolation of low-p_T physics. At higher p_T, the jets start to matter; the jet cross-section in this region is given at least approximately by the lowest order QCD formula built in ISAJET, and so our sample should contain about the right mixture of low-p_T and soft jet events.

For technical reasons, we have divided the minimum bias sample into two parts, generating 2000 events with 3 GeV $< p_T <$ 20 GeV and 500 events with 20 GeV $< p_T <$ 100 GeV. We have superimposed on each gluino event and each background QCD jet event, a Poisson distributed number of these minimum bias events corresponding to the luminosity per bunch crossing ($\mathcal{L}_{bunch}$). This implictly assumes that all elements of the detector have good time resolution, so that interactions from different bunch crossings can be separated. When the minimum bias sample is exhausted, we start again at the beginning. We believe that the pile-up of a single missing p_T event with several minimum bias events is in fact the dominant pile-up effect. However, we have not studied in any detail, other possibilities, such as the pile-up of two QCD events each containing a missing p_T ν.

Four different cases of pile-up luminosity have been considered, namely: $\mathcal{L}_{bunch}$ = 0, 0.01, 0.025, and 0.05 mb^{-1}, corresponding respectively to no pile-up, 2, 5, and 10 pile-up events. Our conclusion is that obviously, with pile-up added things get considerably worse, in the following way (Fig. 15); at $\mathcal{L}_{bunch}$ of 0.1 mb^{-1} (which means 2 extra pile-up events) it is still all right; at a pile-up luminosity of 0.025 mb^{-1} the background slope is still within error bars of that with no pile-up. But at $\mathcal{L}_{bunch}$ = 0.5 mb^{-1} (which means 10 extra pile-up events), the signal is significantly degraded. At that point we are faced, in our study, with the problem of having not enough background statistics to decide if the signal could be extracted. It probably could be, but it might not be very convincing and anyhow we already can conclude at this level that with up to 5 extra pile-up events per signal event, we can survive, with our x_{out} cut technique; whereas 10 pile-up events make life really hard, if not impossible. Of course apart from the x_{out} scheme, one can think of applying a p_T threshold on each calorimeter cell already at the first level trigger; this reduces the pile-up a lot but how much does it also bias our physics output at a very preliminary stage? (In particular how much does it bias a first-level trigger?)

IVc. SUSY vs. Background

We summarize in Table 3 all the different backgrounds other than that from light constituent jets which can affect our search for SUSY particles. It includes not only the standard model background (SU(2) × U(1)), but also possible signals coming from new physics which can mimic SUSY. For each case, we have given, for different mass ranges, the corresponding cross section as well as the ratio of signal over background (S/B). Most of the cross sections quoted in the table are from EHLQ. We see that for $\tilde{g}\tilde{g}$ and $\tilde{g}\tilde{q}$ the backgrounds other than light constituent jets are not severe. For $\hat{g}\tilde{\gamma}$ production the background from $p \to Z$ + jet, $Z \to \nu\bar{\nu}$ swamps the signal. However, the situation will be improved by applying an E_t missing cut and an x_{out} cut. Similarly, the background to $\tilde{g}\tilde{w}$ production from $pp \to W$ + jet; $W \to e\bar{\nu}$ is severe but will be reduced by E_t missing cuts.

In conclusion, the background due to light quark constituents, in particular, is important, especially in the case of the $\tilde{g}$ pair production or $\tilde{g}\tilde{q}$ production. The x_{out} technique seems to be better than a simple E_T^{miss} cut to handle this problem as well as the pile-up effect, at least up to 5 extra events superimposed on top of the signal events. At a level of 10 pile-up events the situation becomes much more critical, and more sophisticated studies (including higher statistics) need to be pursued to be sure whether or not we can survive in such conditions. The other backgrounds, in general, are less critical; but anyhow a more refined definition of the characteristics of the SUSY events is needed to ensure their signature.

V. Recommendations for a SUSY Trigger

At this stage of our work, we want to extract some characteristics of the SUSY events we are looking at, in terms of certain calorimetric information. Our ambition is to use them to build a "SUSY trigger". By trigger we mean in fact all the different levels of selection, from the first-level hardware trigger to higher levels such as the ones including on-line processors. The data selected in this way, already on-line, would be registered on special records (for "express-line" analysis).

To perform this analysis, we use the same tools (jet finder, simulation program, etc.) as defined in Section III. For the different SUSY reactions we are concerned with, we have studied the total transverse energy (E_T) spectra of the event, the inclusive jet distribution, the missing energy as well as the total number of jets reconstructed in each event using our simple jet algorithm, the transverse energy of the highest E_T jet and of the lowest E_T jet. We have summarized the results obtained in Table 4 giving for all these quantities, the corresponding average value.

From what is listed in this table as well as the results already obtained in Sections III and IV, we can give the following list of "recommandations" for defining a SUSY trigger.

Recommendation No 1:

A "SUSY trigger" must be a *multipurpose SUSY tester*; this means that, in order to be sure to overcome both pile-up and all the kinds of backgrounds we already mentioned, we must take advantage of the fact that SUSY proposes a list of reactions, some with rather high cross-section, but more difficult to identify [reactions (1) and (2)] others with lower cross-section but cleaner signal [such as reactions (3) and (4)].

Recommendation No. 2:

An x_{out} cut must be applied: it will certainly help in beating the light constituent background as well as the pile-up.

Recommendation No. 3:

The requirement on the jet topology must be included very soon in the trigger; using the Lego plot technique, and a simple jet finder it is possible to get the number of jets of the events.

Recommendation No. 4:

The jet topology requirement must be combined with a cut on the E_T^{miss}.

Recommendation No. 5:

Some specific trigger bits can be defined such as for instance:

i) A "$\tilde{g}\tilde{\gamma}$ trigger bit" including a simple jet topology (one or two nearby jets) *and* a p_T imbalance in the event just back to back with the "monojet".

ii) A "$\tilde{W}\tilde{g}$ trigger bit" including a simple jet structure (two or three jets) and an isolated high E_T electron and a very large missing energy at least $\geq$ O (70%) the highest E_T jet.

Table 3. SUSY vs. Background at $\sqrt{s}$=40 TeV.

Process			Standard Model Background	Confusion with Minimal Extention				Confusion with Technicolor Models	
$pp\to\tilde{g}\tilde{g}$			$pp\to W^+W^-$ $\frac{S}{B}=\frac{\sigma(pp\to\tilde{g}\tilde{g})}{\sigma(pp\to W^+W^-)}$	$pp\to Q\bar{Q}$ $R=\frac{\sigma(pp\to\tilde{g}\tilde{g})}{\sigma(pp\to Q\bar{Q})}$		$pp\to W'^{\pm}X$ $R'=\frac{\sigma(pp\to\tilde{g}\tilde{g})}{\sigma(pp\to W'X)}$		$pp\to P_8P_8$ $R''=\frac{\sigma(pp\to\tilde{g}\tilde{g})}{\sigma(pp\to P_8P_8)}$	
$m_{\tilde{g}}$(TeV)	σ(nb)			m_Q=.5 TeV	m_Q=1 TeV	$m_{W'}$=.5 TeV	$m_{W'}$=1 TeV	m_{P_8}=.24 TeV	m_{P_8}=.5 TeV
.1	50		S/B~1000	R~1000	R~25000	R'~60	R'~360	R''~16	R''~500
.25	6		S/B~120	R~120	R~3000	R'~8	R'~40	R''~2	R''~60
1	.02		S/B~.2	R~.2	R~5	R'~.01	R'~.1	R''~.003	R''~.1
$pp\to\tilde{g}\tilde{q}$			$pp\to W^+W^-$ $\frac{S}{B}=\frac{\sigma(pp\to\tilde{g}\tilde{q})}{\sigma(pp\to W^+W^-)}$	$pp\to Q\bar{Q}$ $R=\frac{\sigma(pp\to\tilde{g}\tilde{q})}{\sigma(pp\to Q\bar{Q})}$		$pp\to W'^{+}X$ $R'=\frac{\sigma(pp\to\tilde{g}\tilde{q})}{\sigma(pp\to W'X)}$		$pp\to P_8P_8$ $R''=\frac{\sigma(pp\to\tilde{g}\tilde{q})}{\sigma(pp\to P_8P_8)}$	
$m_{\tilde{g}}$ (TeV)	$m_{\tilde{q}}$ (TeV)	σ (nb)		m_Q=.5 TeV	m_Q=1 TeV	$m_{W'}$=.5 TeV	$m_{W'}$=1 TeV	m_{P_8}=.24 TeV	m_{P_8}=.5 TeV
.1	.1	15	S/B~300	R~300	R~7000	R'~20	R'~100	R''~5	R''~150
.25	.25	2	S/B~40	R~40	R~1000	R'~3	R'~15	R''~.7	R''~20
1	1	.01	S/B~.2	R~.2	R~5	R'~.01	R'~.1	R''~.003	R''~.1
$pp\to\tilde{g}\tilde{\gamma}$			$pp\to ZX;Z\to\nu\bar{\nu}$ $\frac{S}{B}=\frac{\sigma(pp\to\tilde{g}\tilde{\gamma})}{(.2)\,\sigma(pp\to ZX)}$	$pp\to L\nu_L;L\to q\bar{q}\nu_L$ $R=\frac{\sigma(pp\to\tilde{g}\tilde{\gamma})}{(.7)\sigma(pp\to L\nu_L)}$					
$m_{\tilde{g}}$ (TeV)	$m_{\tilde{\gamma}}$ (TeV)	σ (nb)		m_L=.5 TeV	m_L=1 TeV				
.1	.1	7×10^{-3}	S/B~10^{-3}	R~40	R~300				
.25	.25	10^{-3}	S/B~3×10^{-4}	R~5	R~40				
1	1	10^{-5}	S/B~3×10^{-6}	R~.05	R~.4				
$pp\to\tilde{g}\tilde{W}$; $\tilde{W}\to e\bar{\nu}\tilde{\gamma}$			$pp\to W^{\pm}X;W\to e\nu$ $\frac{S}{B}=\frac{\sigma(pp\to\tilde{g}\tilde{W})}{(.1)(pp\to WX)}$	$pp\to L^+L^-;L^+\to q\bar{q}\bar{\nu}_L$ $L^-\to e\bar{\nu}\nu_L$ $R=\frac{\sigma(pp\to\tilde{g}\tilde{W})}{(.07)\,(pp\to L^+L^-)}$					
$m_{\tilde{g}}$ (TeV)	$m_{\tilde{W}}$ (TeV)	σ (nb)		m_L=.5 TeV	m_L=1 TeV				
.1	.1	2×10^{-2}	S/B~5×10^{-3}	R~9000	R~6×10^4				
.25	.25	4×10^{-3}	S/B~10^{-3}	R~1500	R~10^4				
1	1	7×10^{-5}	S/B~2×10^{-5}	R~30	R~230				

* We have specifically excluded the background from light constituents from this table as this background is treated elsewhere. All cross sections are from EHLQ[3] with cuts on the rapidities of the produced particles of $|y_i|<1.5$. W' is a heavy W with identical coupling as the standard W, P_8 is an octet techniboson (which decays to tb), Q is a heavy quark, L is a heavy lepton and ν_L is its associated neutrino (presumed massless). For the purposes of illustration, we have assumed B.R.($Z\to\Sigma\nu\bar{\nu}$)=.2, B.R.($L\to q\bar{q}\nu_L$)=.7, B.R.($L\to e\bar{\nu}\nu_L$)=.1, B.R.($W\to e\nu$)=.1, B.R.($W\to e\bar{\nu}\tilde{\gamma}$)=1, and B.R.($\tilde{g}\to q\bar{q}\tilde{\gamma}$)=1.

Table 4 Parameters of SUSY events at $\sqrt{s}$ = 40 TeV

Process	Masses (GeV)	$<E_t^{Missing}>$ (GeV)	$<E_t^{total}>$ (GeV)	<# of jets>	$<E_t^{fast\ jet}>$ (GeV)	$<E_t^{slow\ jet}>$ (GeV)
$pp \to \tilde{g}\tilde{g}$	$m_{\tilde{g}} = 100$	47	208	2	87.5	59.4
$\tilde{g} \to q\bar{q}\tilde{\gamma}$	$m_{\tilde{g}} = 1000$	424	1467	4	688	181
$pp \to \hat{g}\tilde{\gamma}$	$m_{\tilde{g}} = 100$					
$\hat{g} \to q\bar{q}\tilde{\gamma}$	$m_{\hat{q}} = 500$	63.4	99	1	69	66.5
$pp \to \tilde{g}\tilde{q}$	$m_{\tilde{g}} = 500$					
$\tilde{g} \to q\bar{q}\tilde{\gamma}$	$m_{\hat{q}} = 200$	187	557	3	267	109
	$m_{\tilde{g}} = 200$					
	$m_{\hat{q}} = 500$	114	600	4	248	81
$pp \to \tilde{W}\tilde{g}$	$m_{\tilde{W}} = 200$					
$\tilde{g} \to q\bar{q}\tilde{\gamma}$	$m_{\tilde{g}} = 200$	118	303	2	159	87.2
$\tilde{W} \to e\hat{\nu}$	$m_{\tilde{W}} = 1000$	534	1373	3	739	265
$\hat{\nu} \to \nu\tilde{\gamma}$	$m_{\tilde{\gamma}} = 1000$					

*** In all cases, we have considered the photino to be massless and stable.**

These special triggers have, in addition, the advantage of giving a *signal* even in the case where the sparticles are of relatively low mass (too low to be identified in other processes such as $\tilde{g}\tilde{g}$ or $\tilde{g}\tilde{q}$ at SSC energies but too high to be identified in the previous set of machines).

In the next section we study the effect of varying the detector definition in our simulation.

VI . Detector Simulation

We now want to go a step further. We are pushing the sparticles we have generated with ISAJET through "real" detectors. We have considered for this two cases; in one case we simulate a "classical" 4π detector à la CDF; in the other case a 4π detector which is purely a calorimeter "à la D1" [see Calorimeter and 4π Detector Group Studies at this meeting[13]].

VIa. Simulation of SUSY Events Through a "CDF Type" 4π Detector

We say that this detector is classical, in the sense that it includes a central part which is a tracking device, surrounded by e.m. and hadronic calorimetry and then muon chambers. A solenoidal field of 15 kG is applied. The events generated with ISAJET are submitted to the CDF detector simulation program. The CDF apparatus has been "adapted" to a 40 TeV machine; the calorimetry geometry is that of CDF but with the density of the hadronic calorimeter doubled. We, therefore, have 1 interaction length of e.m. calorimeter and 10 interaction lengths of hadronic calorimeter. The e.m. part is lead-scintillator and the hadronic part resembles a uranium scintillator detector. The pseudorapidity range covered by the apparatus is ± 5. The interaction point is centred within a value of σ = 5 cm along the beam axis. A 15 kG solenoidal field is present. Resolution and detector tracks are included, giving in particular a more realistic picture of the missing energy spectrum. Infortunately, the CDF tracking routine was not yet available at the time we did this work, so this part of the information is still missing.

The jets are located using a fairly simple cluster finder. A cluster seed threshold is used to define a minimum energy for a cluster to be initiated in a given tower. This seed threshold was set at 2 GeV for all runs except two for which it was 5 GeV. The finder then searches the nearest neighbours picking up anything above 100 MeV. It does some searching for valleys to determine if two or more clusters are touching. The clusters are then checked to see if they can be merged. Clusters whose centres have $\Delta r = \sqrt{(\Delta\eta)^2 + (\Delta\phi)^2}$ less than 1.0 are merged, the merged clusters being the jets.

For each type of SUSY process studied, we give the following distributions: total E_T of the event, missing E_T, total number of jets in the event, invariant mass of jet pairs, inclusive jet E_T spectrum, E_T of the largest E_T jet, E_T of the lowest E_T jet (Figs. 16–18), and some Lego plots of SUSY events as seen from the CDF experiment (Figs. 19–21). By looking at the corresponding pictures we see that the main conclusions we have drawn in Section IV are still valid and confirmed when we use another jet finder and another apparatus simulation.

We can give more specific comments; in the case of $\tilde{g}$ pair production, for $m_{\tilde{g}} = 100$ GeV, the number of jets is 2 to 4 (Figs. 8a, 11a), as expected $q,\bar{q}$jets tend to merge and thus many events are with 2 or 3 rather than 4 jets. If $m_{\tilde{g}} = 1$ TeV, it gives 3 to 5 jets per event (Figs. 16a, 19b) and less merging of $q\bar{q}$ jets (at least as far as the jet algorithm is concerned); the total E_T distribution tends to peak near the mass of single $\tilde{g}$ (Fig. 16a). Missing E_T is not so spectacular (Fig. 16a). In the case of $\tilde{g}\tilde{\gamma}$ production, we studied two values for the gluino mass: 100 GeV and 1 TeV. The effect of merging appears quite clearly as one goes to lower mass (Figs. 17a, 20). When 2q-jet coming from the $\tilde{g}$ decay dissociates into 2 distinct jets, we also note that one is much higher in transverse energy than the other one (Figs. 17c, 20). The scatter plot of the missing transverse energy as a function of the transverse energy of the jets is essentially populated along the diagonal (Fig. 17d); so a rather good $p_T$imbalance characterized this type of reaction. For the $\tilde{g}\tilde{W}$ production, the number of jets is 2 to 4 depending on the mass range of the sparticles (Figs. 18a, 21). Additional information about the e^- is given in Fig. 18b: even thin shower counters typically see 90% of the electron energy.

VIb. Simulation of SUSY Events through a 4π D1 type Detector.

The idea in this section is to use a simulation package built by the Detector Study Group and flexible enough to incorporate different hypotheses on geometry, granularity, and material. So SUSY events can be plugged in such an apparatus simulation as a typical example of new physics and allows us to get a better feeling about the performances required for the calorimeters we need for the next generation machine.

To do so, we have modelled the response of a purely calorimetric detector similar in design to the D1 detector described in these Proceedings (see report of the Detector Study Group). A schematic view of the detector is shown in Fig. 22. It consists of five cylindrical sections, one central (CC), two end caps (EC), and two end plugs (EP), all with projective tower geometry. Each tower is segmented into two layers in depth and has an angular coverage of 50 mrad in azimuth (2.8°) and 0.05 units in rapidity η. The material has a 1 cm radiation length and a hadronic absorption length, λ of 20 cm. The CC covers the angular region $24.5° < \theta < 155.5°$ (or $-1.525 < \eta < 1.525$), where θ is the angle with respect to the beam axis. It has a total thickness of 10 λ (1 λ and 9 λ segments). The ECs extend the coverage down to 5.56° ($\eta = 3.025$) on each side and have a total thickness of 11 λ (1 λ and 10 λ segments). Finally the EPs go down to 0.277° from the beam ($\eta = 6.025$) and have a total thickness of 12 λ (1 λ and 11 λ segments). The total length of the detector is about 15 m.

The following processes were studied for this case:

$pp \to \tilde{g}\tilde{g}$,	$\tilde{g} \to q\bar{q}\tilde{\gamma}$,	$m_{\tilde{g}} = 100$ GeV,
$pp \to \tilde{g}\tilde{g}$,	$\tilde{g} \to q\bar{q}\tilde{\gamma}$,	$m_{\tilde{g}} = 1$ TeV,
$pp \to \tilde{g}\tilde{q}$,	$\tilde{g} \to q\bar{q}\tilde{\gamma}$,	$m_{\tilde{g}} = 200$ GeV,
	$\tilde{q} \to q\tilde{g}$,	$m_{\tilde{q}} = 500$ GeV,
$pp \to \tilde{g}\tilde{q}$,	$\tilde{g} \to q\bar{q}\tilde{\gamma}$,	$m_{\tilde{g}} = 500$ GeV,
	$\tilde{q} \to q\tilde{\gamma}$,	$m_{\tilde{q}} = 200$ GeV.

These processes give multijet type events which are of interest in this work. They allow analysis of the required structure of calorimeters. These detectors have to be able to recognize even tricky multijet structure where jets can sometimes be close to one another. Electromagnetic showers and hadronic cascades were simulated with the programs developed for the Fermilab Collider D^0 detector[13]. This gives as output the energy deposited in each calorimeter cell. A simple jet-finding algorithm (similar to the one described in Section III) was developed to reconstruct the events.

Figure 23 shows a Lego plot of the energy distribution for a typical gluino pair event where the gluino mass is taken to be 1 TeV.

The same distributions as the ones discussed in Section V have been looked at and very similar results obtained (see, for instance, Fig. 24). In addition, the background of light constituents has been simulated through this D1 apparatus prototype and some distributions (Fig. 25) of the general characteristics of these events show that this background looks different from the $\tilde{g}$ pair signal at least if the $\tilde{g}$ mass is large enough [$\gg$ O(500 GeV)].

Of course, we have not studied all the possible alternatives that can be figured out for the definition of (for instance) a detector for SSC; but, we have set up, for the first time, a tool, namely the simulation of SUSY events through different apparatus. This can be of great use for the future. Even if SUSY would be a relatively low mass scale physics (already accessible with present generation machines), it can be used as a *prototype* of new physics; its specific requirements concerning jet recognition, missing energy, or lepton identification are typically the ones of any other kind of physics we can imagine (at least at the moment!) beyond the standard model.

By examining the results we obtained in the case both of a "classical" or a "calorimetric" 4π detector, we can already point out the main following requirements:

- HERMITICITY = 4π detector with as few CRACKS as possible.
- FINE SEGMENTATION to identify between $(q\bar{q})$, $(qq\bar{q})$ and q or g jet structure and be as sensitive as possible to the "merging effect" (present at relatively low masses).
- LEPTON IDENTIFICATION for vetoing certain backgrounds, to recognize e's (needs also a magnetic field) or μ's in the case of certain SUSY signatures.
- TRACKING: this is not yet proved in our present report because the tracking package was not available in our simulation à la CDF; so it is more a personal bias, but a very strong one, of some of us based on personal experience at the present $p\bar{p}$ Collider.
  Even if it is very hard at 40 TeV, tracking is certainly a very important tool as far as SUSY is concerned.

To study, in more detail, what physics requires as the best granularity for a calorimeter, the exact performances of a tracking device, the trigger pattern, the on-line processing, etc. goes much beyond the purpose of our study group (see its title!); but the tool has been built and we have started to use it with these goals in mind.

VII. Refined Monte Carlo

How much are the conclusions we have obtained so far affected by the change of the generator package. How much do other reactions fake the detection of some SUSY processes which have even a rather clean signature (such as for instance $\tilde{g}\tilde{\gamma}$ or $\tilde{W}\tilde{g}$ production).

These are the two questions we ask ourselves in this Section. To answer them, we need a more refined Monte Carlo generator. In particular, it should be able to point out in a more reliable way than a simpler generator package peculiar properties of some kinematical or physical distributions.

For these reasons, two of us (R. M. B. and H. H.) have built an event generator for the reactions,

(a) $pp \to \tilde{W}\tilde{g}$ with $\tilde{W} \to q\bar{q}\tilde{\gamma}$ and $\tilde{W} \to e\tilde{\nu}$, $\tilde{\nu} \to \nu\tilde{\gamma}$

(b) $pp \to \tilde{g}\tilde{\gamma}$

This generator is discussed in detail by Barnett and Haber in these proceedings.[14] For reaction (a) we take $m_{\tilde{g}} = m_{\tilde{W}} = 1$ TeV and $m_{\tilde{\gamma}} = 950$ GeV and consider the p_t distribution of the lowest E_t jet, of the highest E_t jet, and of the electron, Fig. (26). We note that the $q\bar{q}$ system coming from the decay of the gluino gives one jet much higher in E_t than the other one, consistent with the results of Sections IV and V. The distributions of the E_t of each jet are rather similar to the ones obtained with ISAJET at the same mass range. The difference in spacial angle between the two jets coming from the gluino decay and between the highest E_t jet and the e^- are shown in Fig. (27). Such quantities could be used to ensure a $\tilde{W}\tilde{g}$ signature.

In Figs. (28) and (29), we show the p_t distributions of the highest E_t jet, of the lowest E_t jet, and of the electron for $m_{\tilde{g}} = m_{\tilde{W}} = 200$ GeV and $m_{\tilde{\gamma}} = 100$ GeV. Figure (28) has a massless photino and Fig. (29) has a 50 GeV photino. The effect of the non-zero photino mass is to shift the peaks of the p_t distributions by about 20 GeV.

For the reaction (b) we show the effect of varying the masses of the sparticles on the distribution of the spacial angle between the two jets coming from the gluino decay. This quantity is quite sensitive to the mass parameter and could be used in a refined analysis. Note that all these results are obtained without any detector simulation.

Certainly such a refined generator will be needed in a careful analysis of some properties of SUSY processes.

VIII. Conclusion

SUSY is the theory for the time when the SSC will be working; NONE of us joined this study group (at least we hope so) with such an idea in mind! What has been our real goal is to use SUSY as a probe to determine the implications that any kind of new physics will have in the design of an apparatus for the SSC machine. To perform this job, we have built new tools or adapted already existing tools such as: Monte Carlo generators, detector simulators, jet finders, etc. This has been made possible also because among all the theories available at the moment on the market, SUSY presents the advantage of being rather well defined; σ's and other parameters are calculated or calculable. At the same time some degrees of freedom are still remaining, such as the mass range and possible different decay scenarios for the sparticles.

It is quite clear that the type of physics we (or the next generation of physicists) will have to study in ten years from now will require highly performing detectors. This statement implies: hermiticity, to measure accurately the p_T imbalance of the events; fine-grained calorimetry including the segmentation in (η, ϕ) to recognize jet topology and internal jet structure and segmentation in depth, to distinguish e^-'s from hadrons; tracking and magnetic field, to specify the jet characteristics, study the amount of neutral over charged component and help in recognizing leptons; μ-identification; trigger and refined on-line processing, allowing the insertion of SUSY signatures at the different levels of selection to prepare already on-line sets of data which could be of interest for this type of physics; High luminosity [$\geq O(10^{32})$] will help as high statistics are needed and beam energy of the order of 20 TeV will allow the scanning of high mass ranges, around 1 TeV range or higher, and also to go down (at least in the case of some reactions) to a few hundred GeV, that is to say to the upper limit that present or next decade machines will reach.

Certainly these studies have to be pursued; we have 10 years to do so!

References

1. I. Hinchliffe and L. Littenberg, in Proceedings of the 1982 DPF Summer Study on Elementary Particle Physics and Future Facilities, edited by R. Donaldson, R. Gustafson, and F. Paige, Fermilab, Batavia, IL, 1982, p.242; S. Aronson, L. Littenberg, F. Paige, I. Stumer, and D. Weyand, *op. cit.*, p. 505; R. M. Barnett, in pp Options for the Supercollider, edited by J. Pilcher and A. White, Chicago,IL, 1984, p. 273.
2. A. Savoy-Navarro, "Experimental Tests of Supersymmetry", Phys. Rep . 105, 91, (1984).
3. E. Eichten, I. Hinchliffe, K. Lane, and C. Quigg, "Supercollider Physics", FERMILAB-Pub-84/17-T, LBL-16875, DOE/ER/01545-345.
4. S. Dawson, E. Eichten, and C. Quigg, "Search for Supersymmetric Particles in Hadron-Hadron Collisions", FERMILAB-Pub-83/82-THY, LBL-16540.
5. H. Haber and G. Kane, "The Search for Supersymmetry: Probing Physics Beyond the Standard Model", UM HE TH 83-17.
6. L. Hall and M. Suzuki, *Nucl. Phys.* *B231*, *419 (1984)*; J. Ellis , in the Proceedings of the 1984 LBL Workshop on Electroweak Symmetry Breaking.
7. P. Harrison and C. Llewellyn Smith, *Nucl. Phys.* *B213*, *223 (1983)*; *B223*, *542 (1983)*.
8. R. M. Barnett and H. Haber, "Detection of Supersymmetric Particles in W-Boson Decay", NSF-ITP-84-78; V. Barger, R. Robinett , W. Keung. and R. Phillips, *Phys. Lett.* *131B*, *375 (1983)*.
9. F. E. Paige and S. D. Protopesch, BNL-29777, Brookhaven, 1983.
10. "CDF Trigger", unpublished internal report of the CDF collaboration, FNAL, 1983.
11. J. Collins et al., report of the QCD group in in these proceedings.
12. S. Ellis et al., report of the Strong Interactions group in these proceedings.
13. Unpublished internal reports of the D0 collaboration.
14. R.M. Barnett and H. Haber, in these Proceedings.

Acknowledgements

We are grateful to E. Eichten, S. Nandi, C. Quigg, and T. Taylor for useful contributions during the course of this work. This work was supported by the Director, Office of Energy Research, Office of High Energy and Nuclear Physics, Division of High Energy Physics of the U.S. Departement of Energy under Contract DU-AC03-76SF00098.

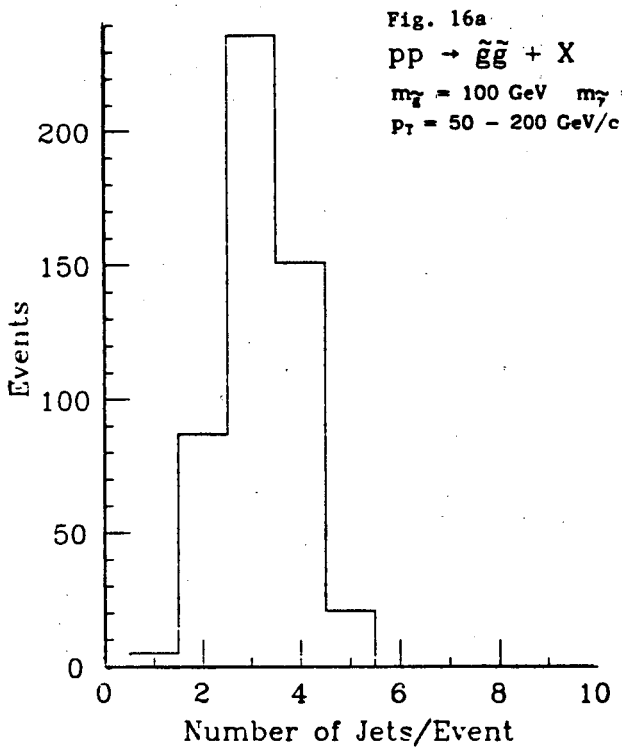
Fig. 16a
pp → g̃g̃ + X
m_g̃ = 100 GeV m_γ̃ = 0
p_T = 50 – 200 GeV/c
Events
Number of Jets/Event

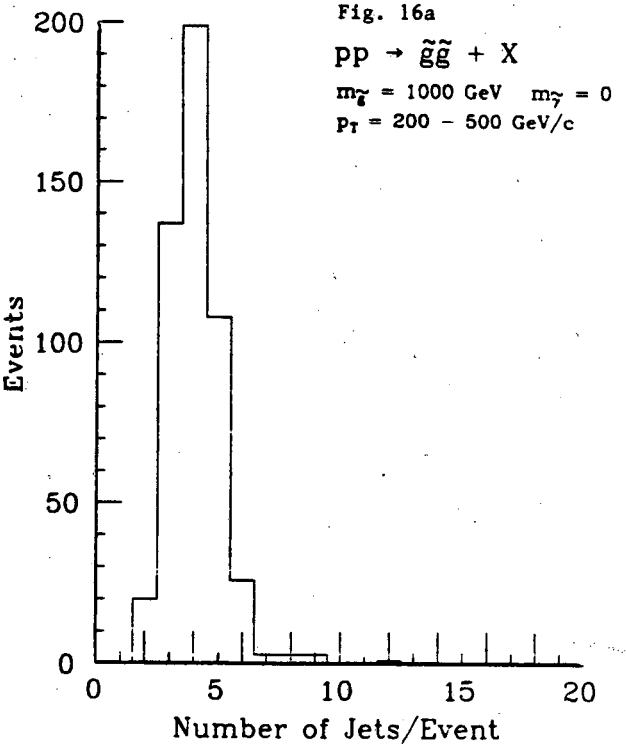
Fig. 16a
pp → g̃g̃ + X
m_g̃ = 1000 GeV m_γ̃ = 0
p_T = 200 – 500 GeV/c
Events
Number of Jets/Event

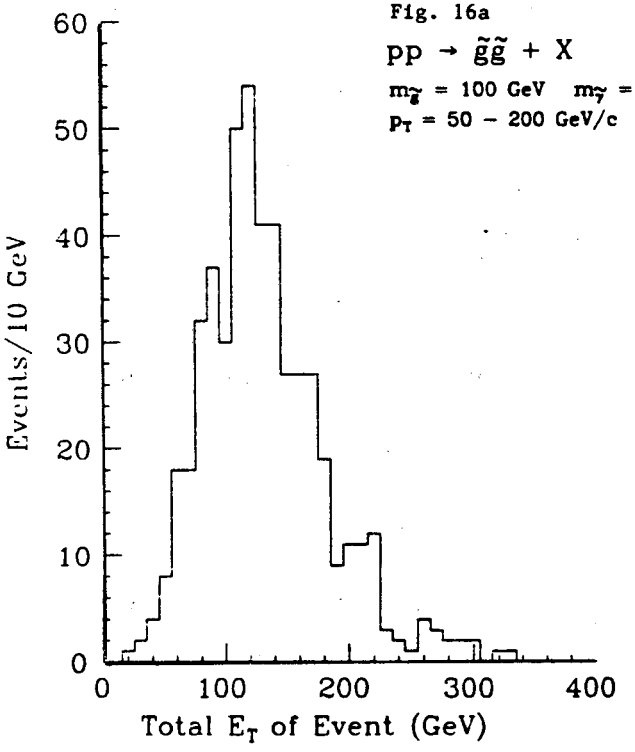
Fig. 16a
pp → g̃g̃ + X
m_g̃ = 100 GeV m_γ̃ = 0
p_T = 50 – 200 GeV/c
Events/10 GeV
Total E_T of Event (GeV)

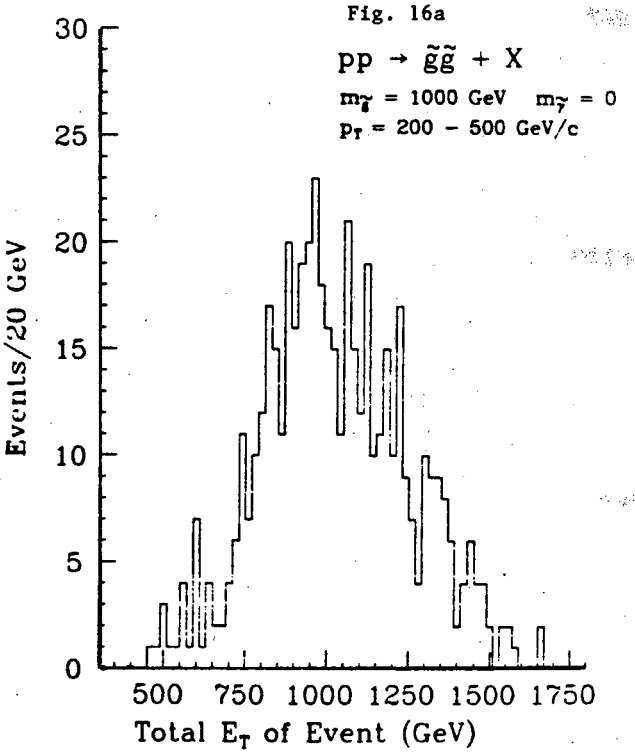
Fig. 16a
pp → g̃g̃ + X
m_g̃ = 1000 GeV m_γ̃ = 0
p_T = 200 – 500 GeV/c
Events/20 GeV
Total E_T of Event (GeV)

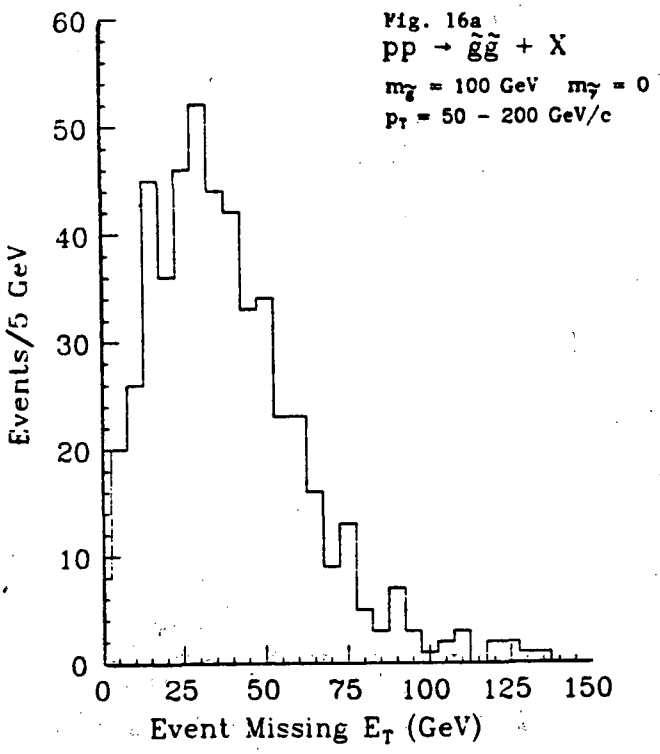

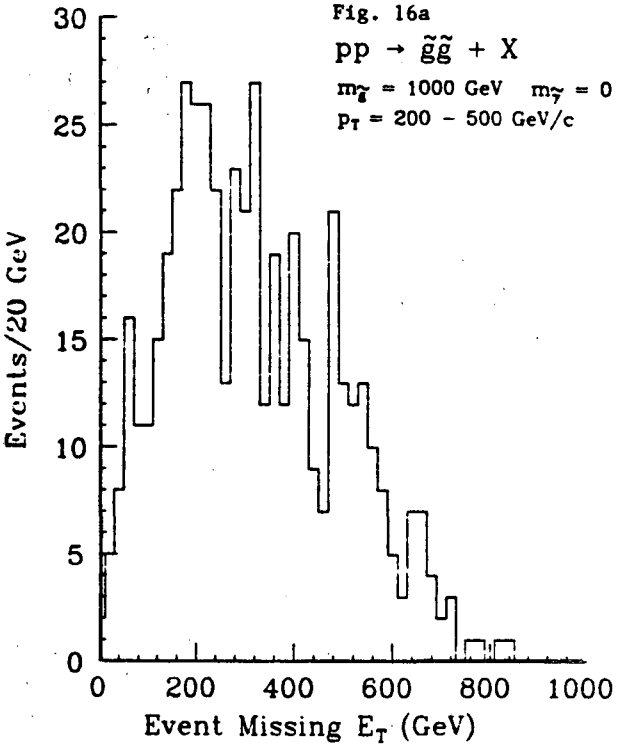

Fig. 16a Event characteristics of the process $pp \rightarrow \tilde{g}\tilde{g}+X$ using the CDF simulation. We have assumed $\tilde{g} \rightarrow q\bar{q}\tilde{\gamma}$, where the $\tilde{\gamma}$ is massless

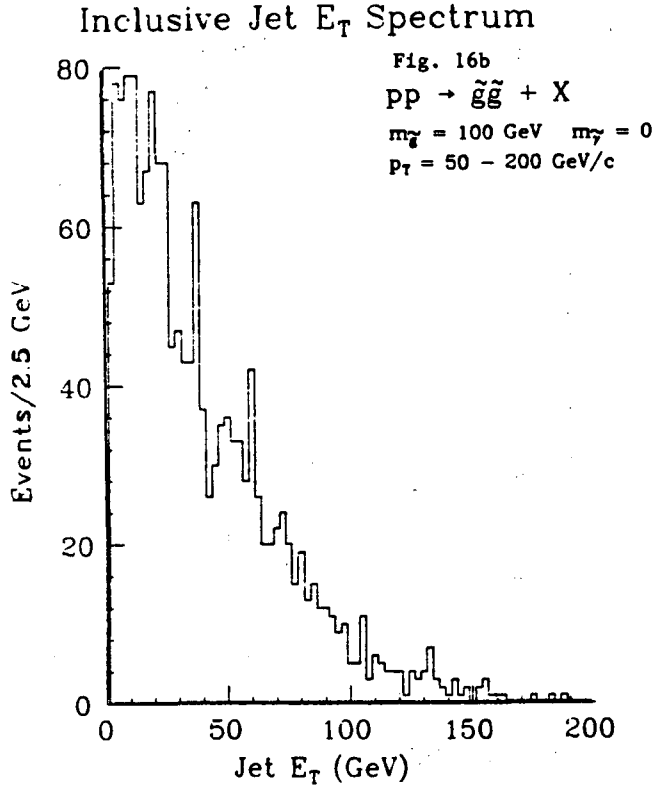

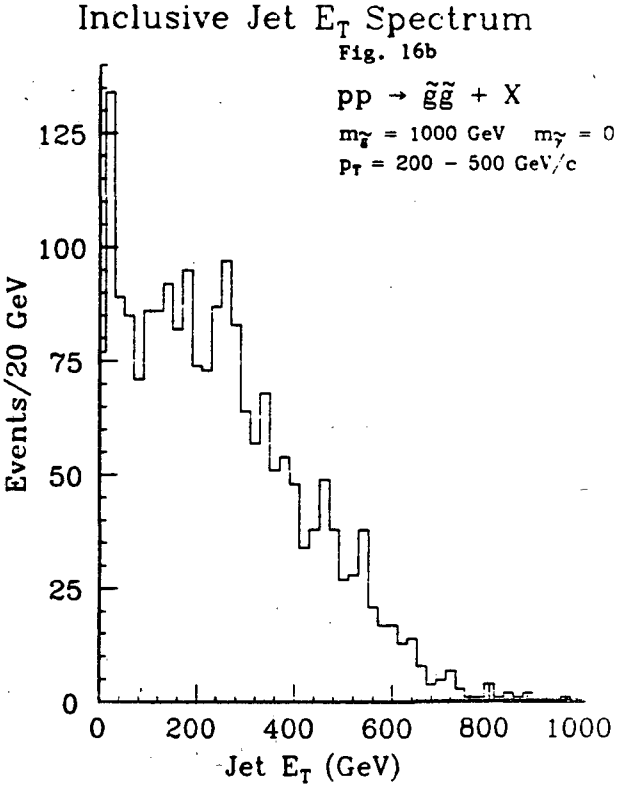

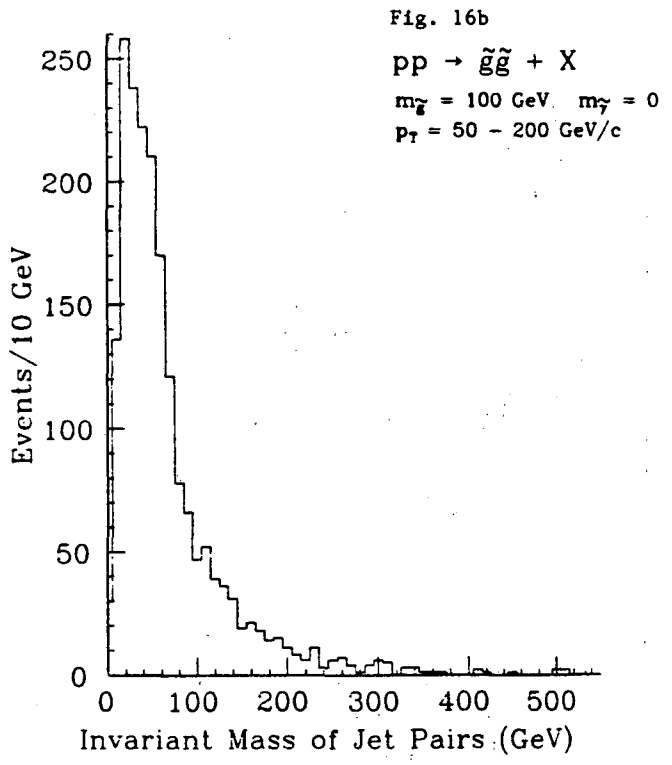

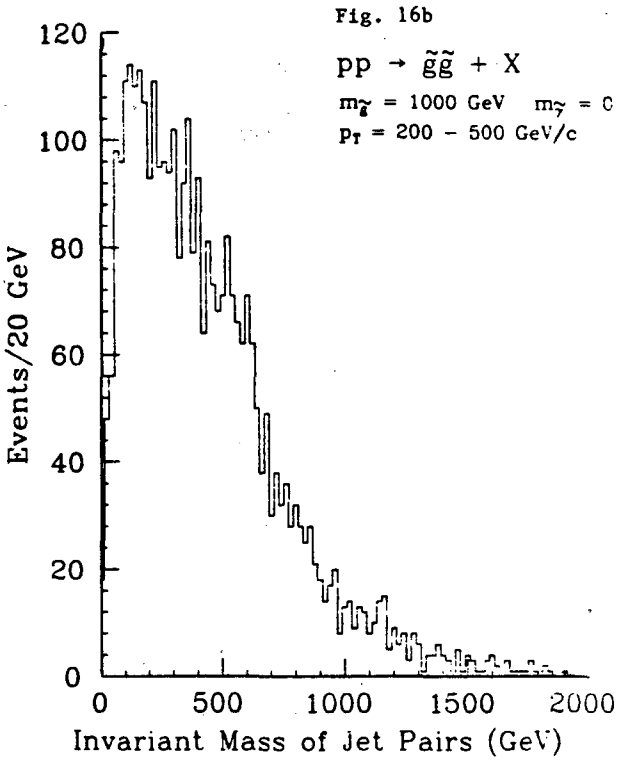

Fig. 16b Jet properties of the process $pp \to \tilde{g}\tilde{g}+X$, using the CDF simulation. We have assumed $\tilde{g} \to q\bar{q}\tilde{\gamma}$ where the $\tilde{\gamma}$ is massless.

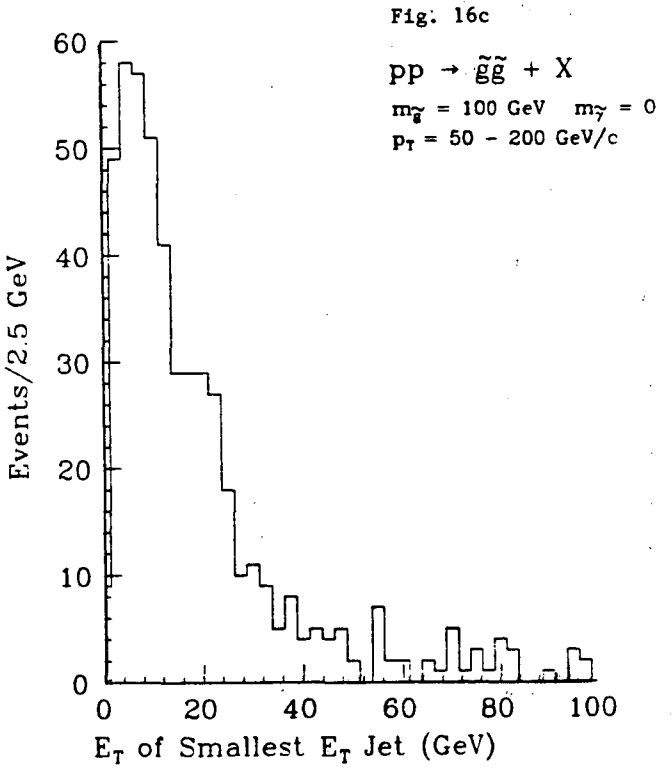

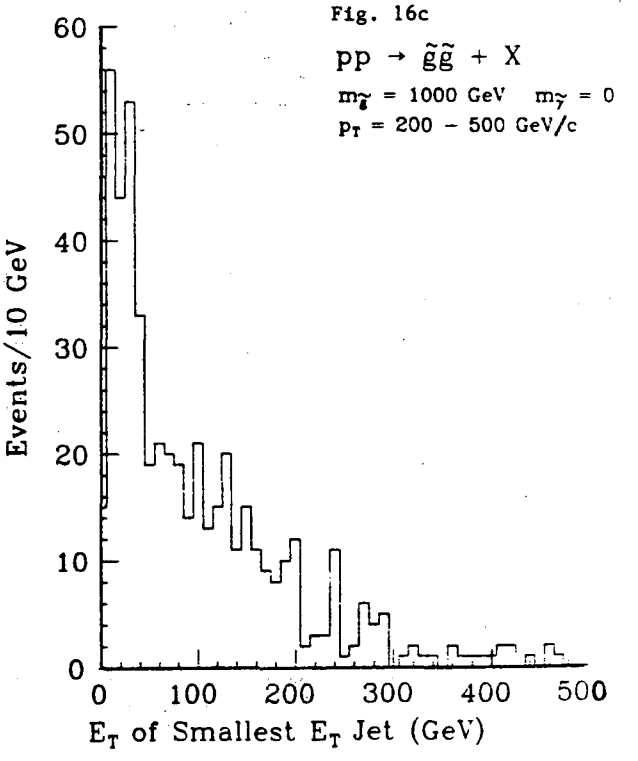

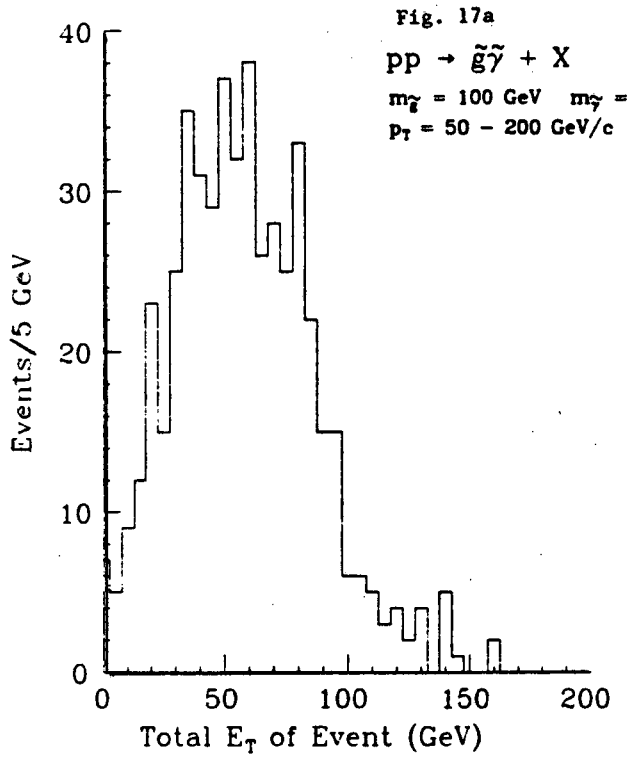

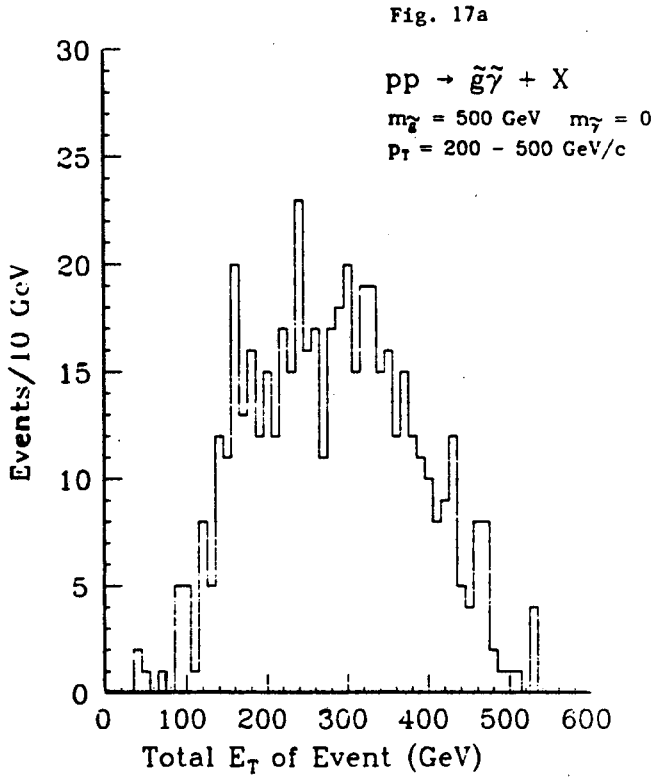

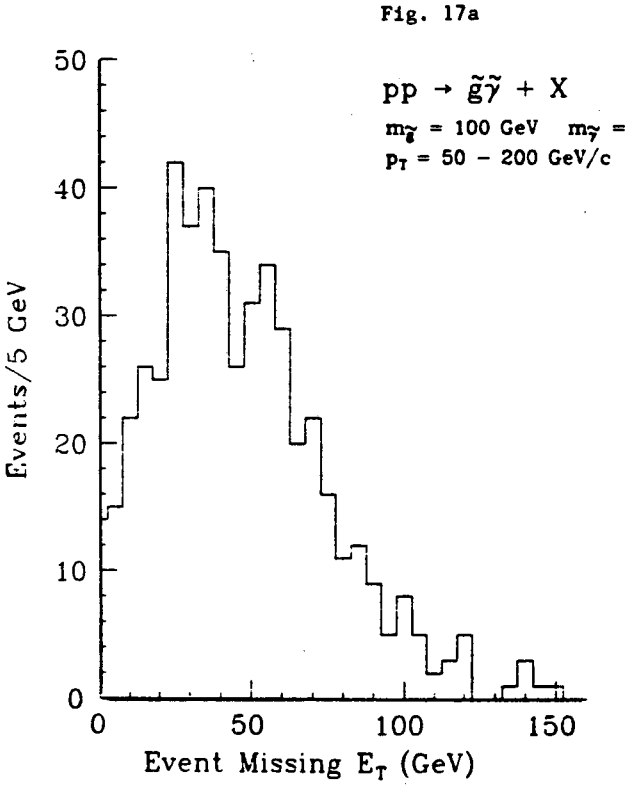

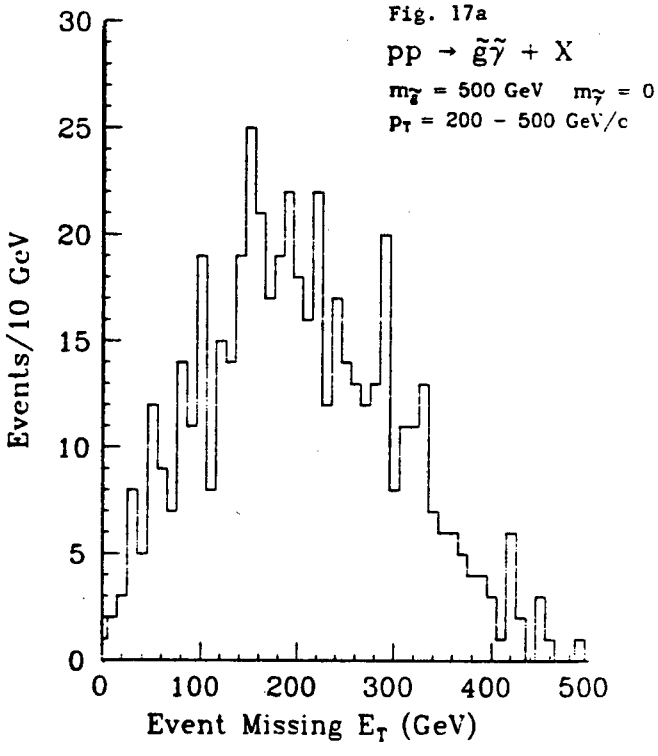

Fig. 17a Event characteristics of the process $pp \to \tilde{g}\tilde{\gamma} + X$, using the CDF simulation. We have assumed $\tilde{g} \to q\bar{q}\tilde{\gamma}$, where the $\tilde{\gamma}$ is massless.

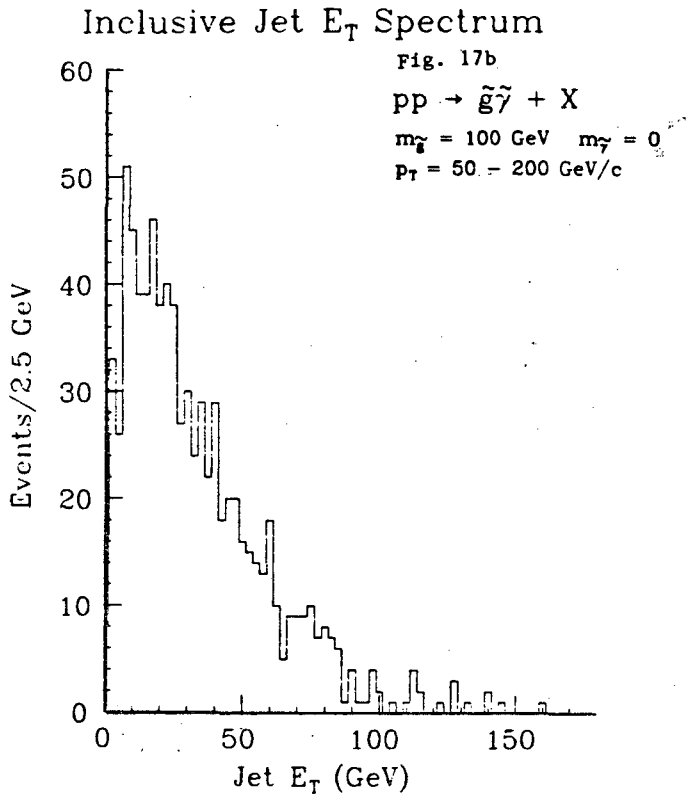

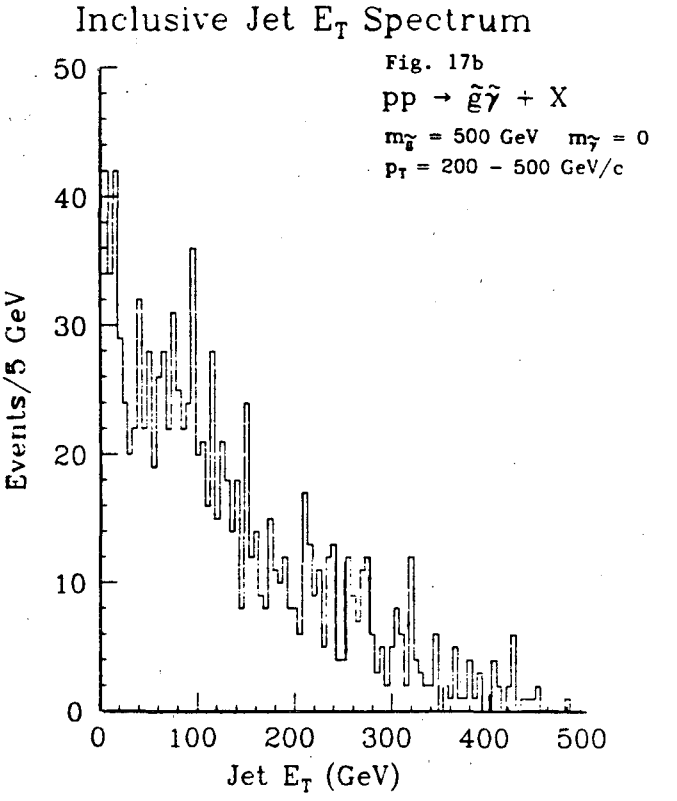

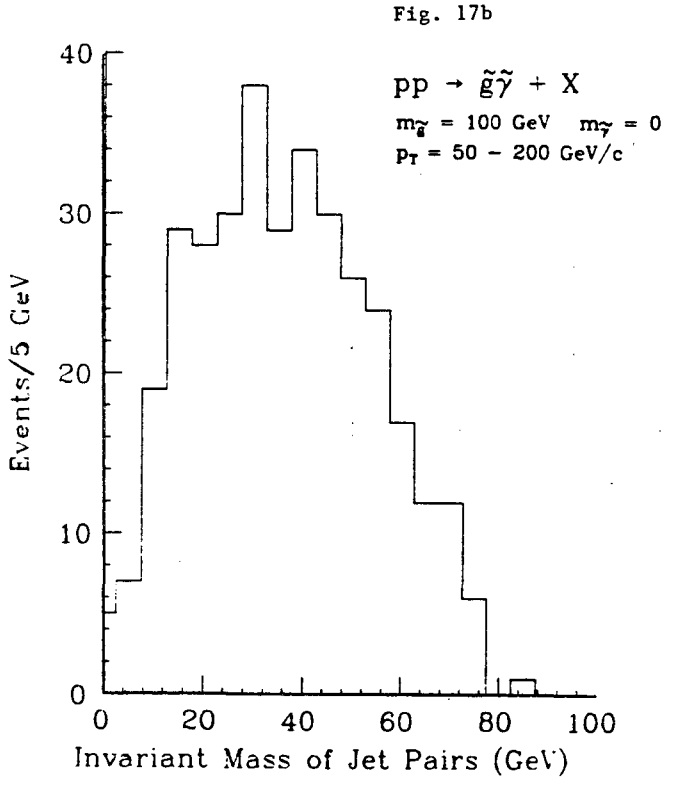

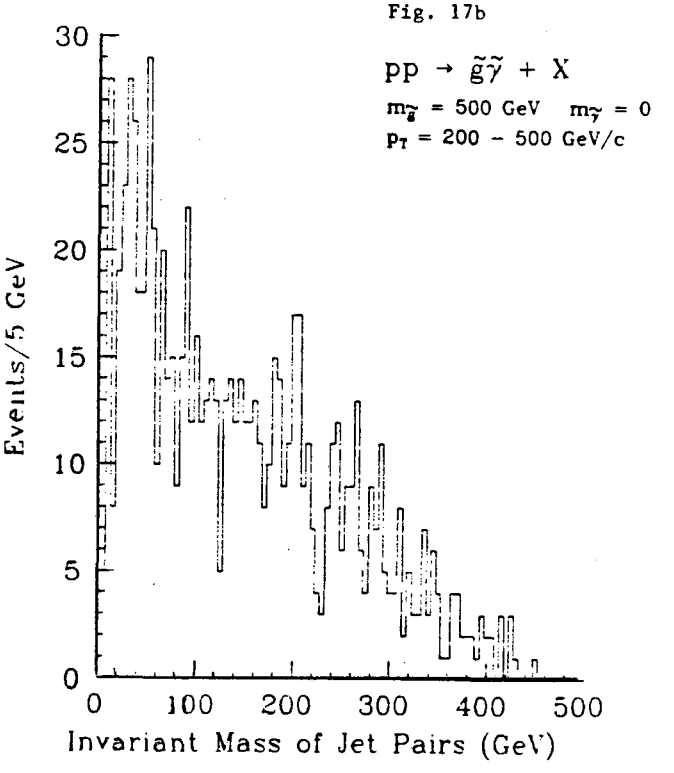

Fig. 17b Jet properties of the process $pp \to \tilde{g}\tilde{\gamma}+X$, using the CDF simulation. We have assume $\tilde{g} \to q\bar{q}\tilde{\gamma}$, where the $\tilde{\gamma}$ is massless.

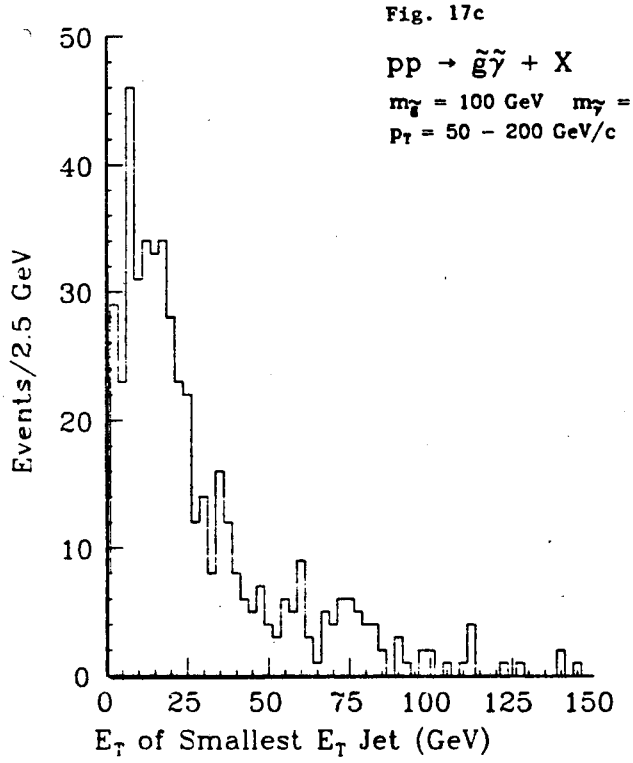

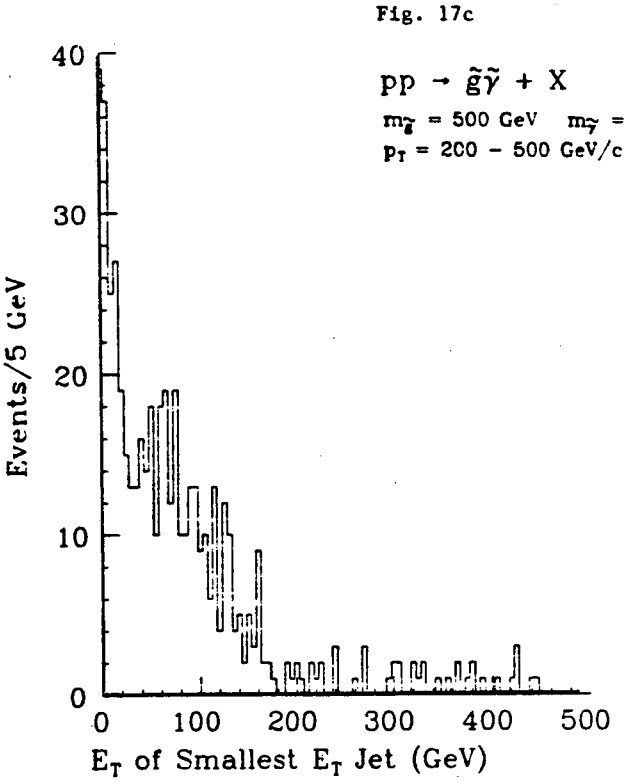

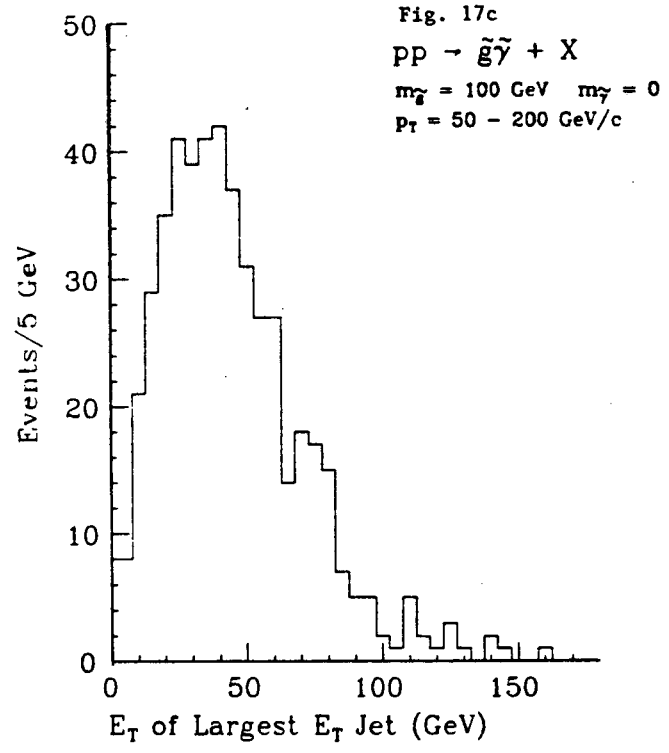

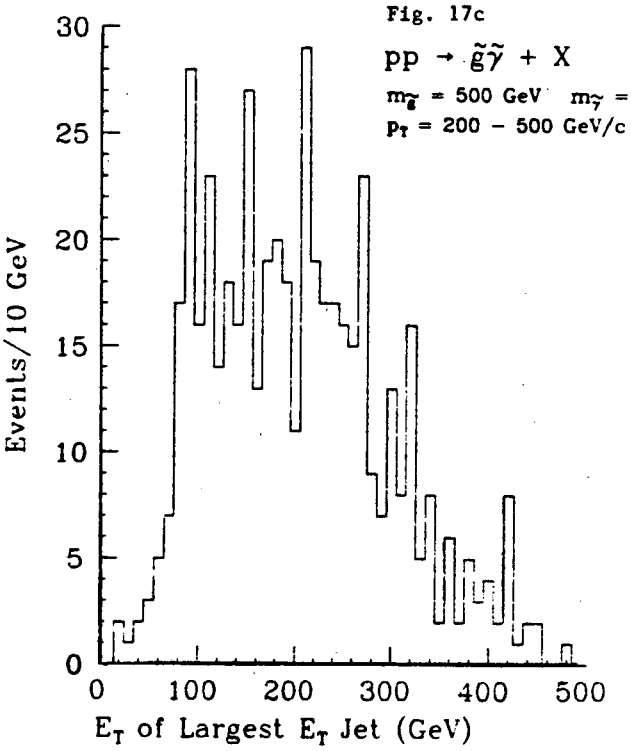

Fig. 17c E_T distribution of smallest and largest E_T jet for the process $pp \to \tilde{g}\tilde{\gamma}+X$, using the CDF simulation. We have assumed $\tilde{g} \to q\bar{q}\tilde{\gamma}$, where the $\tilde{\gamma}$ is massless.

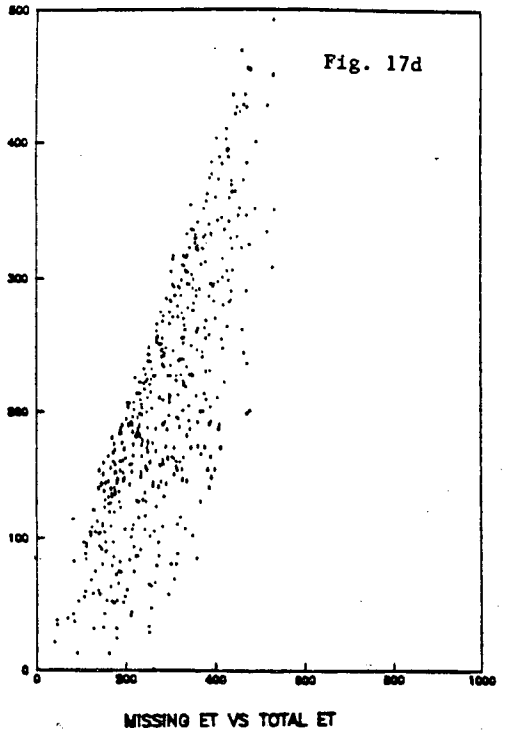

Fig. 17d
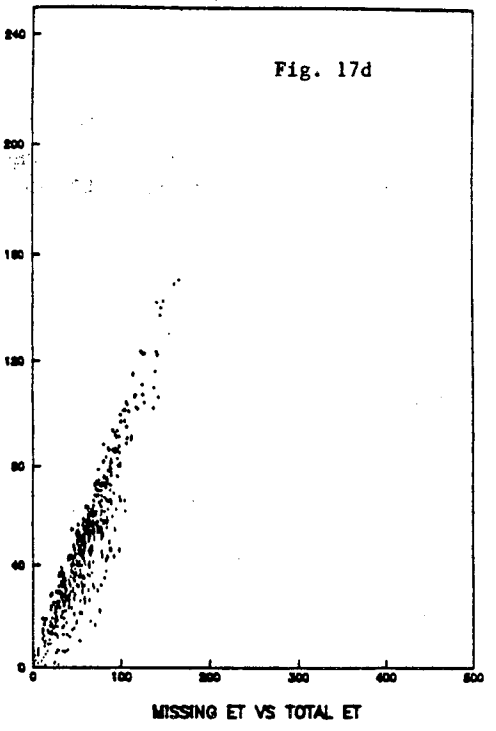

Fig. 17d Missing energy versus total E_T for the process $pp \to \tilde{g}\tilde{\gamma} + X$, using the CDF simulation. We have assumed $\tilde{g} \to q\bar{q}\tilde{\gamma}$, where the $\tilde{\gamma}$ is massless.

Fig. 18a

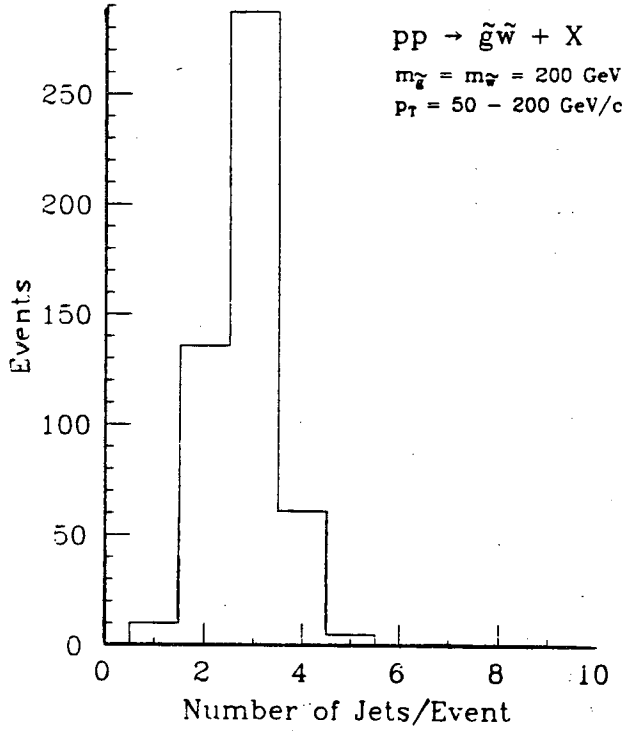

Fig. 18a

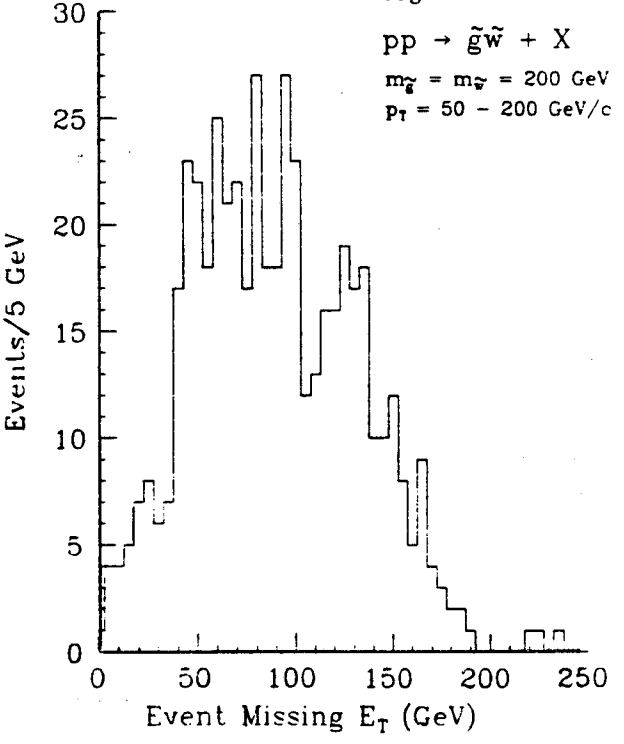

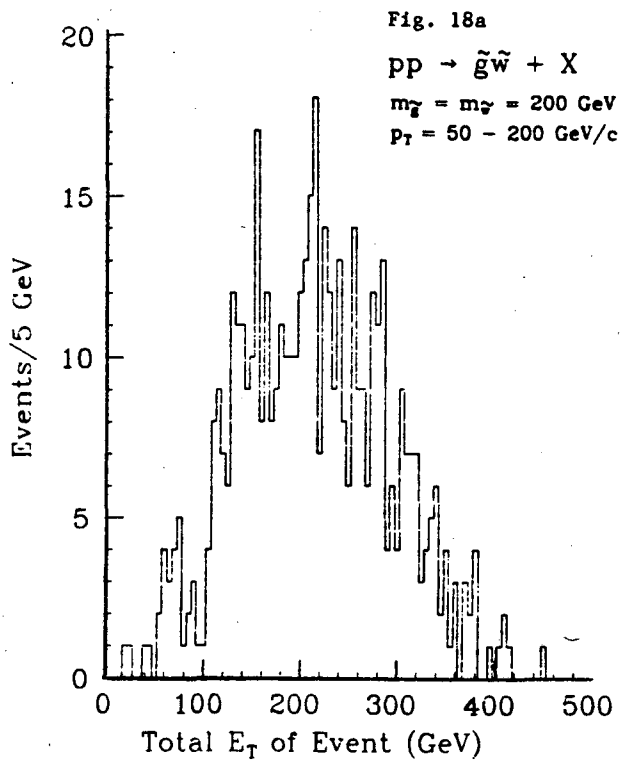

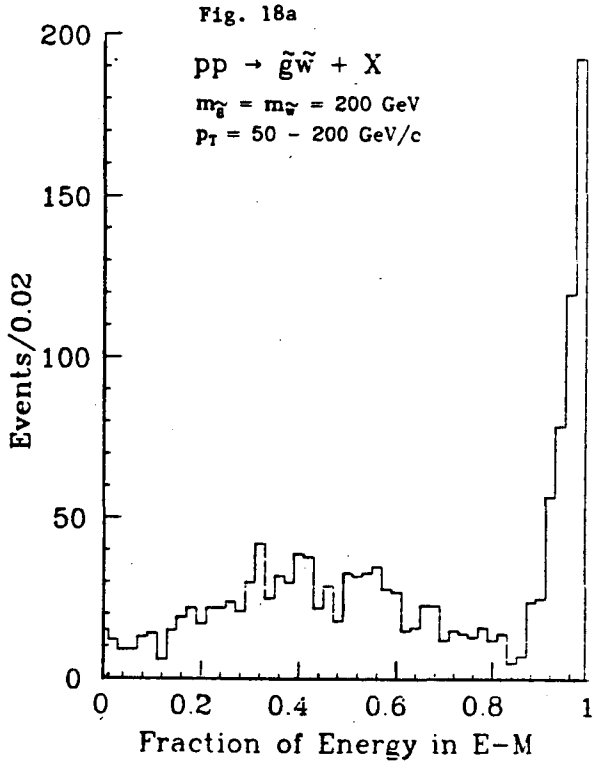

Fig. 18a Event characteristics for the process $pp \to \tilde{w}\tilde{g}+X$, using the CDF simulation. We have assumed $\tilde{g} \to q\bar{q}\tilde{\gamma}$ and $\tilde{w} \to e\nu\tilde{\gamma}$, where the $\tilde{g}$ and the $\tilde{\gamma}$ are massless.

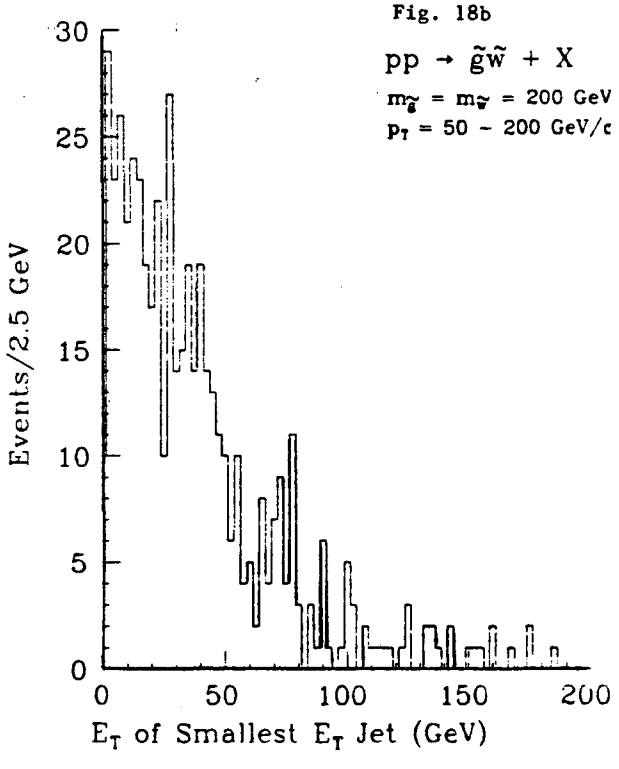

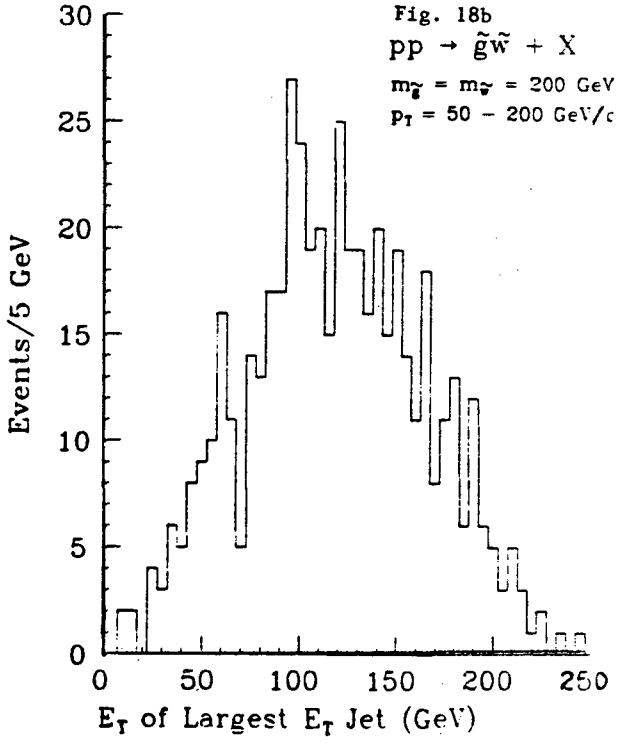

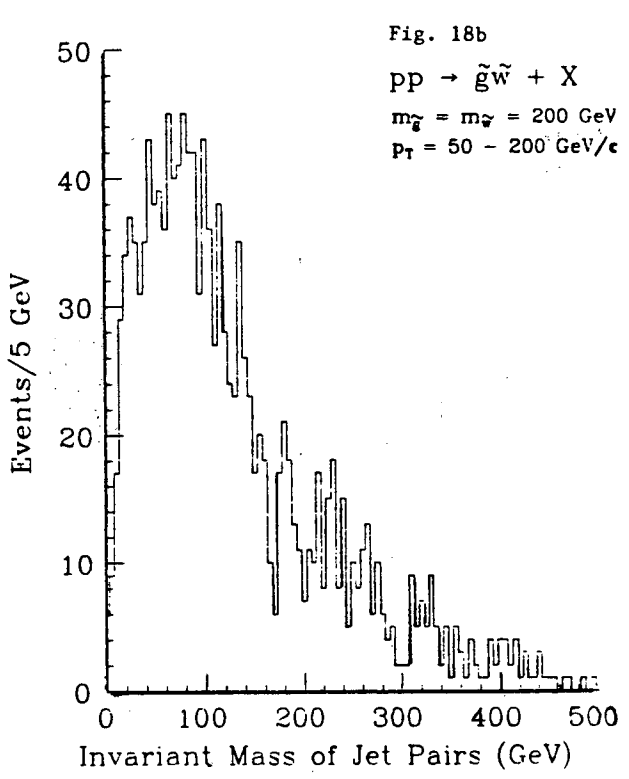

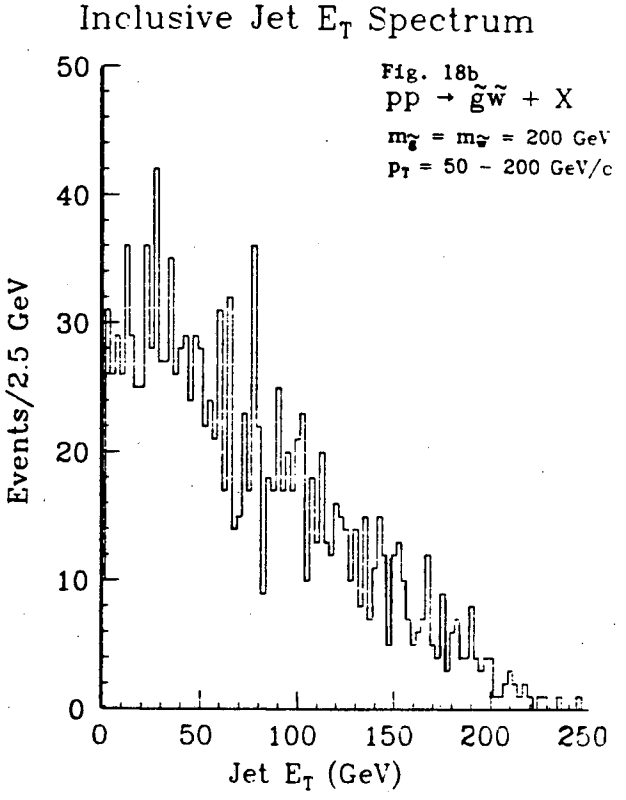

Fig. 18b Jet properties of the process $pp \to \tilde{g}\tilde{w}+X$, using the CDF simulation. We have assumed $\tilde{g} \to q\bar{q}\tilde{\gamma}$ and $\tilde{W} \to e\nu\tilde{\gamma}$, where the $\tilde{\gamma}$ and the $\tilde{\nu}$ are massless.

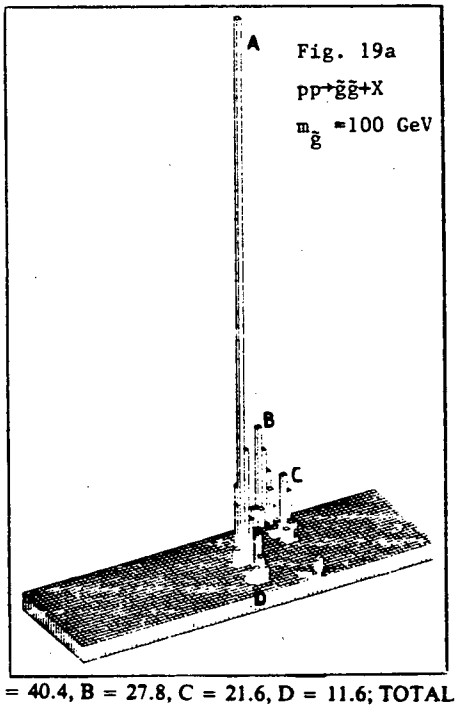

E_T (GeV): A = 40.4, B = 27.8, C = 21.6, D = 11.6; TOTAL = 61.7

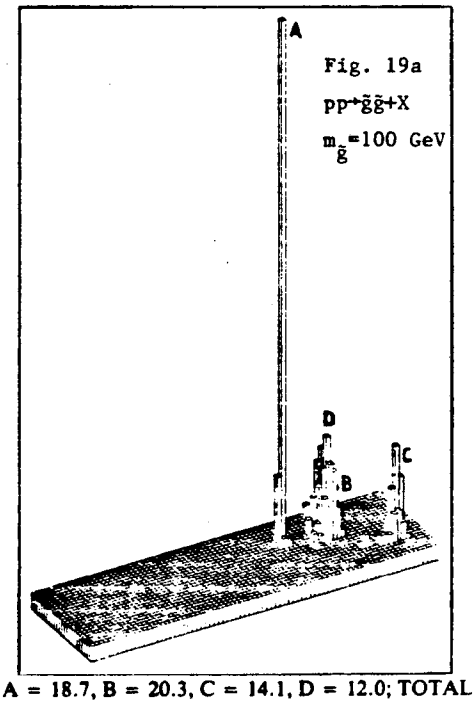

E_T (GeV): A = 18.7, B = 20.3, C = 14.1, D = 12.0; TOTAL = 21.9

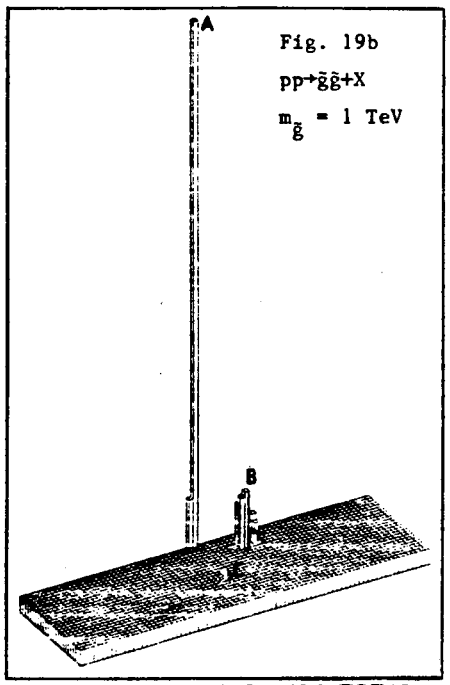

E_T (GeV): A = 459.0, B = 249.3, C = 19.3; TOTAL = 510.4

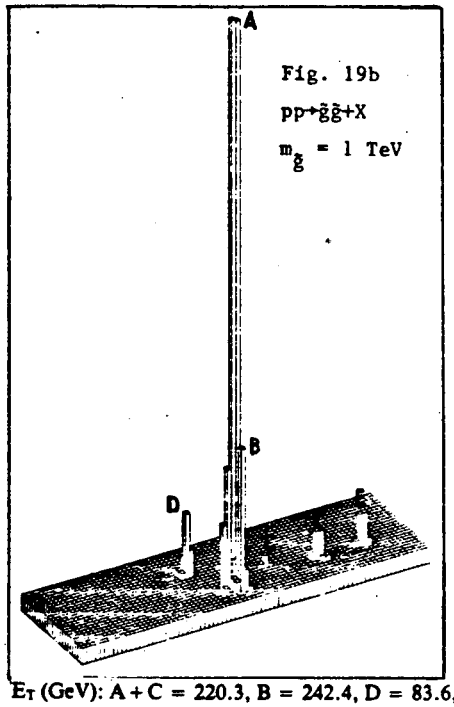

E_T (GeV): A + C = 220.3, B = 242.4, D = 83.6, E = 50.0, F = 41.9; TOTAL = 463.2

Fig. 19 Pictures of pp → g̃g̃ + X events as simulated through the CDF detector, with: a) $m_{\tilde{g}}$ = 100 GeV; b) $m_{\tilde{g}}$ = 1 TeV.

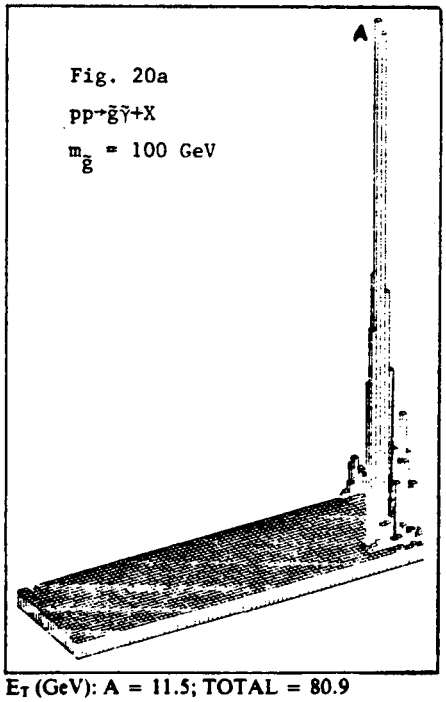

E_T (GeV): A = 11.5; TOTAL = 80.9

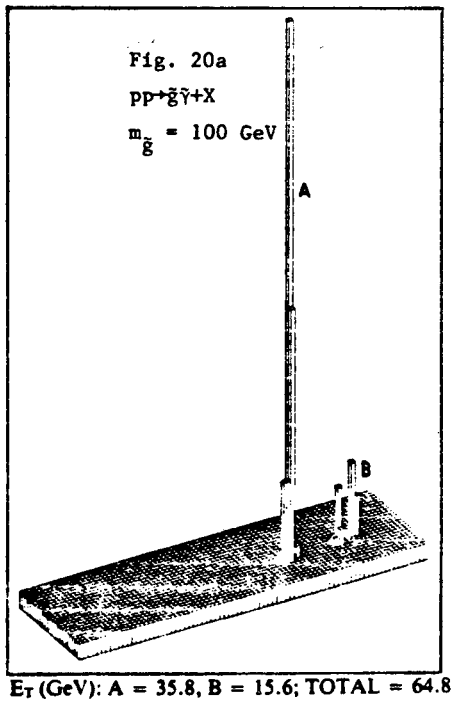

E_T (GeV): A = 35.8, B = 15.6; TOTAL = 64.8

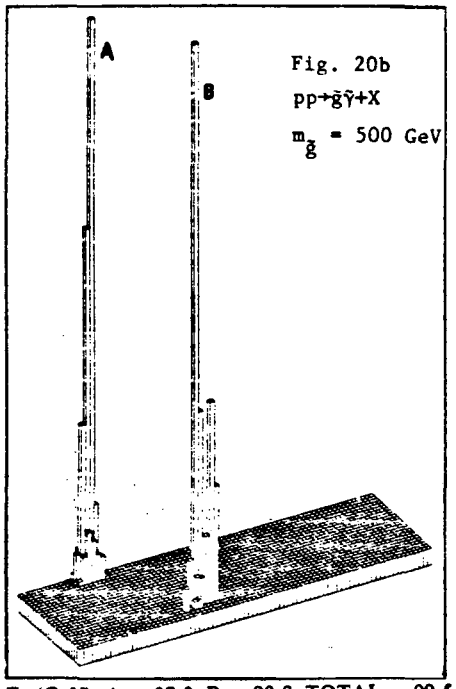

E_T (GeV): A = 37.3, B = 90.8; TOTAL = 99.5

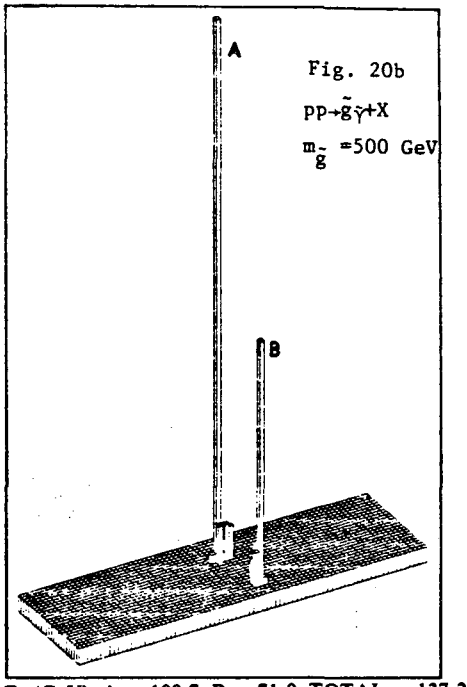

E_T (GeV): A = 108.7, B = 71.0; TOTAL = 137.2

Fig. 20 Pictures of $pp \rightarrow \tilde{g}\tilde{\gamma} + X$ events as simulated through the CDF detector, with: a) $m_{\tilde{g}} = 100$ GeV, $m_{\tilde{\gamma}} = 0$ GeV; b) $m_{\tilde{g}} = 500$ GeV, $m_{\tilde{\gamma}} = 0$ GeV.

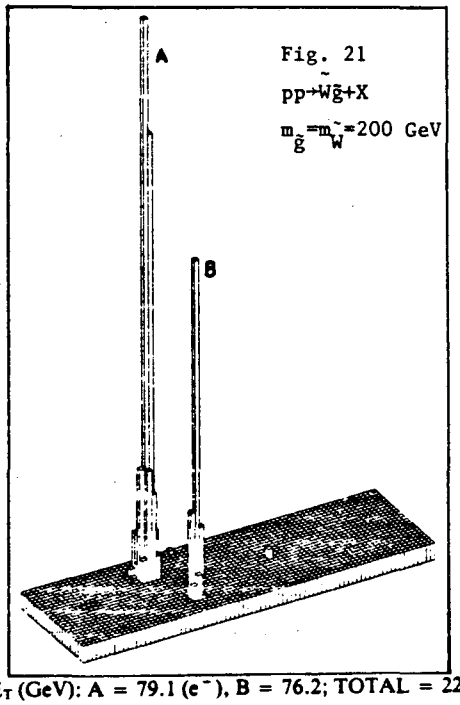

E_T (GeV): A = 79.1 (e^-), B = 76.2; TOTAL = 227.2

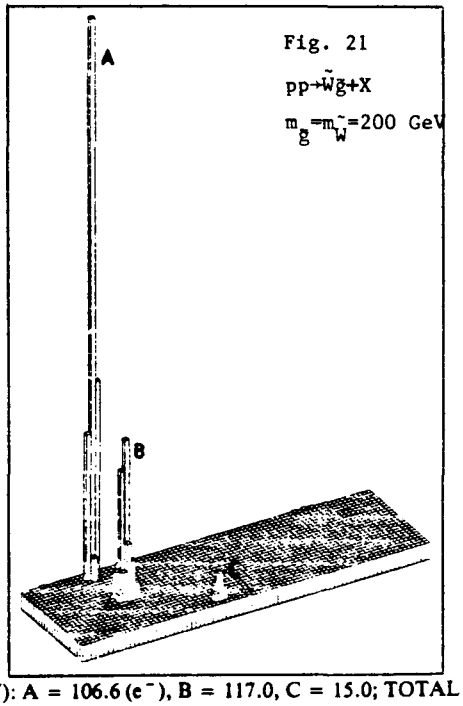

E_T (GeV): A = 106.6 (e^-), B = 117.0, C = 15.0; TOTAL = 177.2

Fig. 21 Pictures of $pp \rightarrow \tilde{W}\tilde{g} + X$ events as simulated through the CDF detector, with $m_{\tilde{g}} = m_{\tilde{W}} = 200$ GeV.

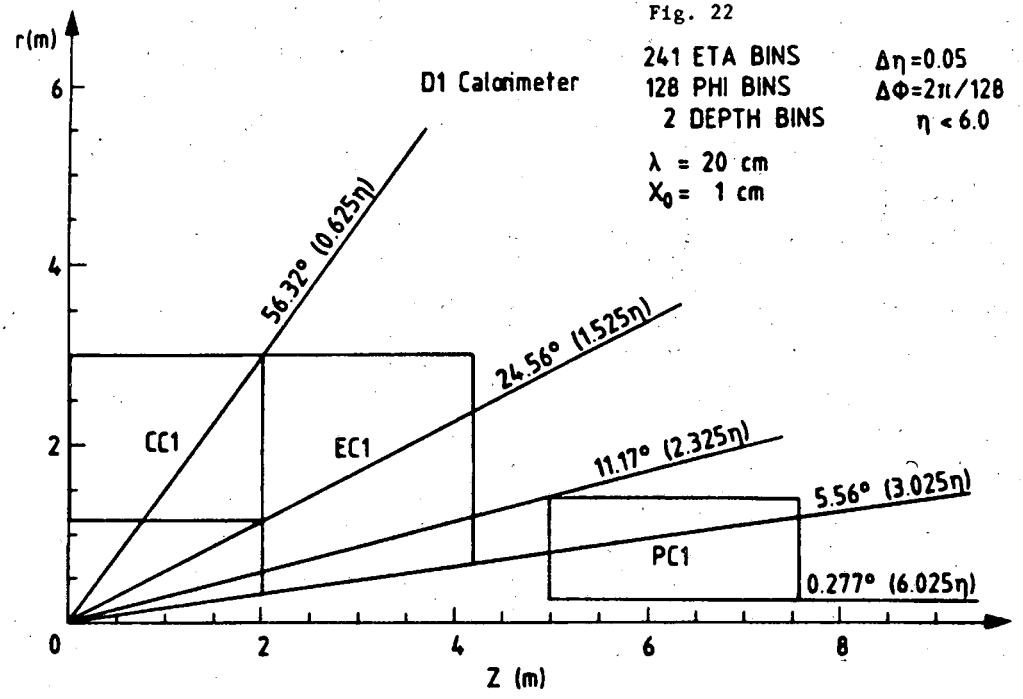

Fig. 22 D1 calorimeter set-up.

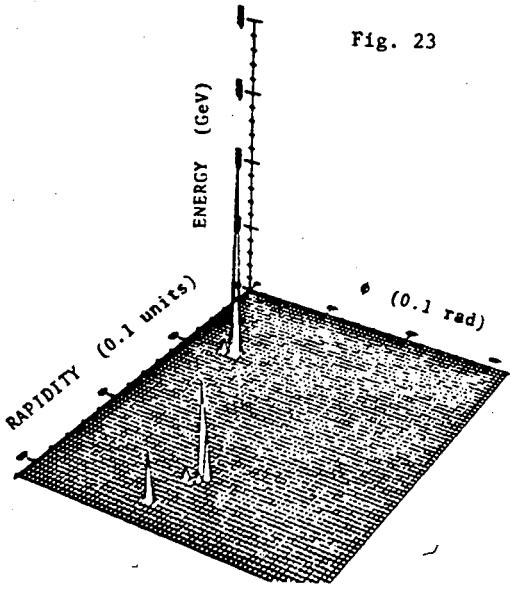

Fig. 23 D1 simulation of $pp \rightarrow \tilde{g}\tilde{g} + X$ ($m_{\tilde{g}}$ = 1 TeV).

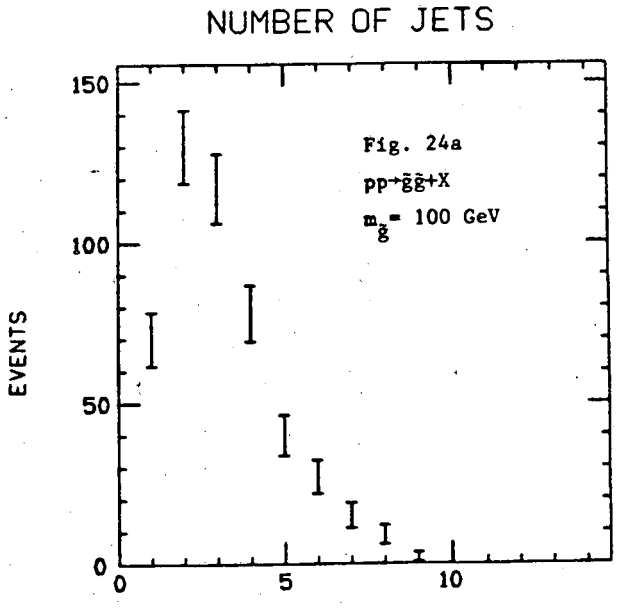

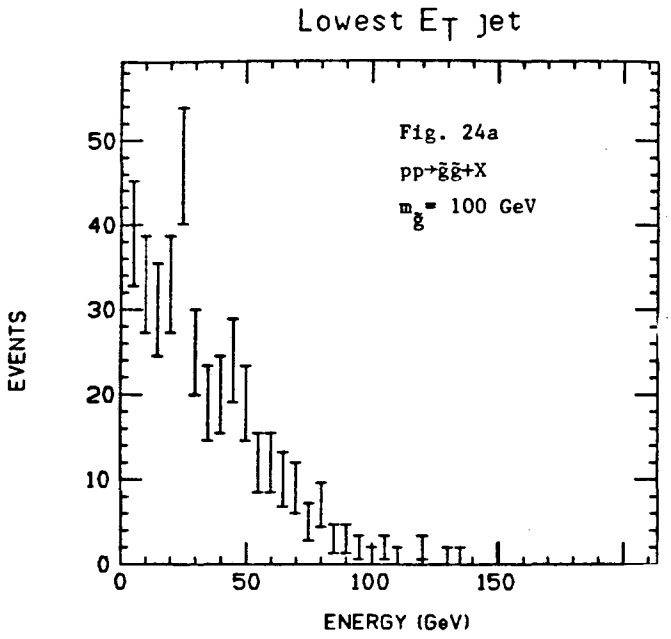

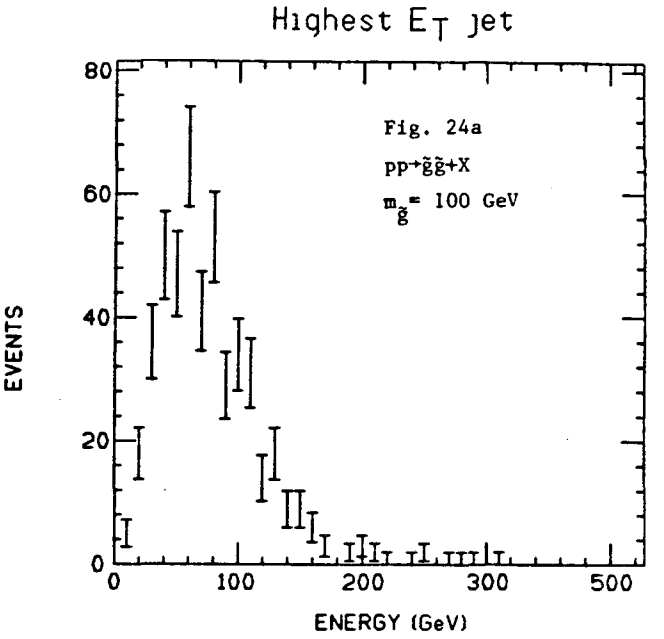

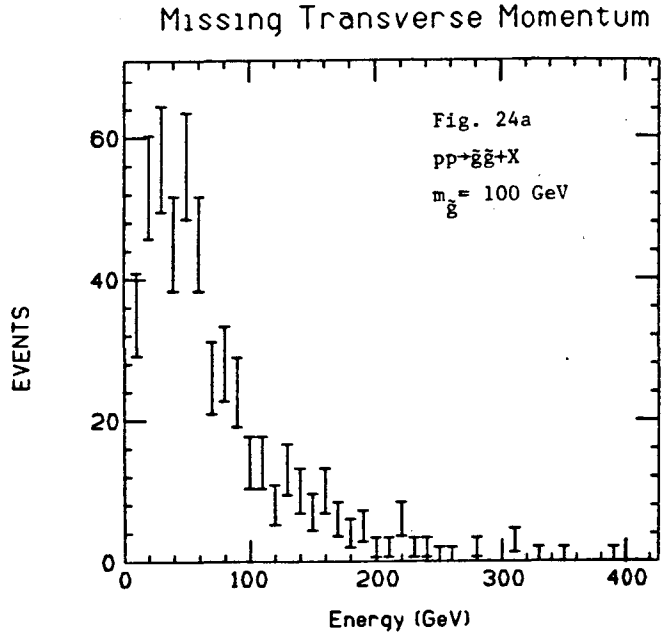

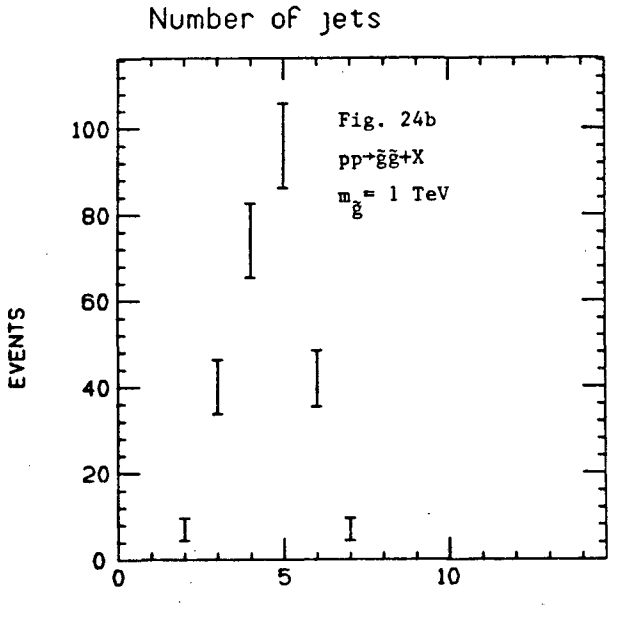

Fig. 24a Event characteristics of gluino pair production simulated through the D1 detector with $m_{\tilde{g}}$ = 100 GeV. We have assumed $\tilde{g}\to qq\tilde{\gamma}$, with $m_{\tilde{\gamma}}$ = 0.

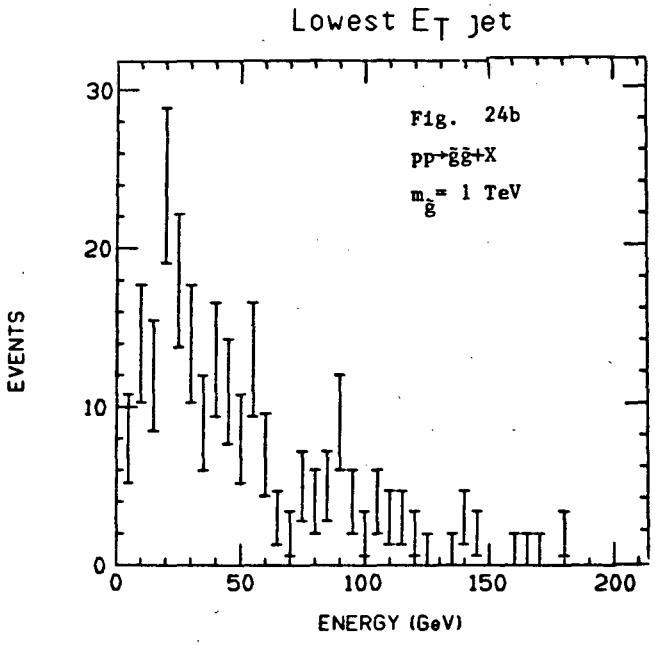

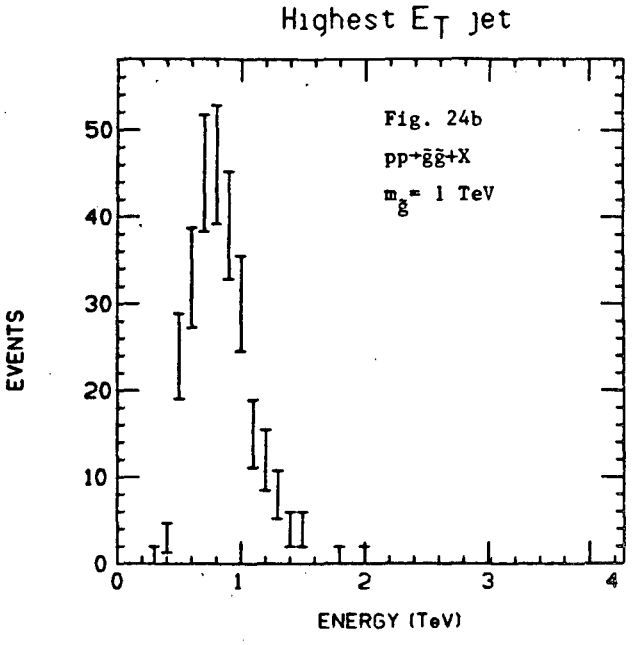

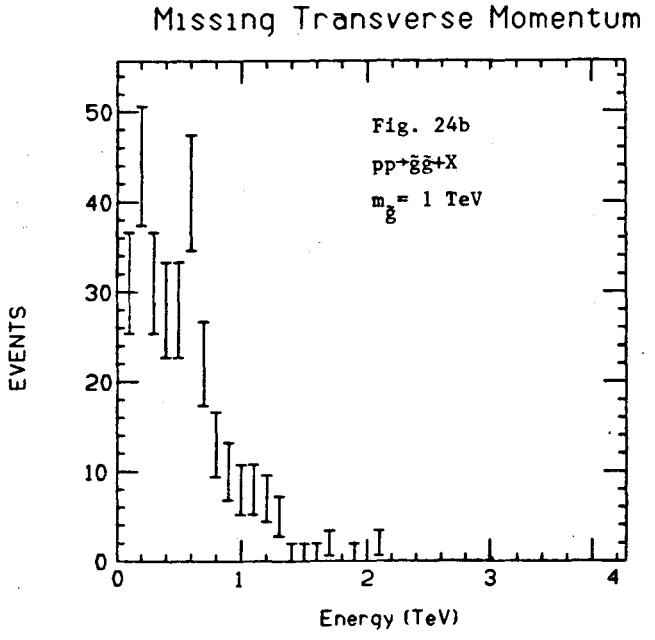

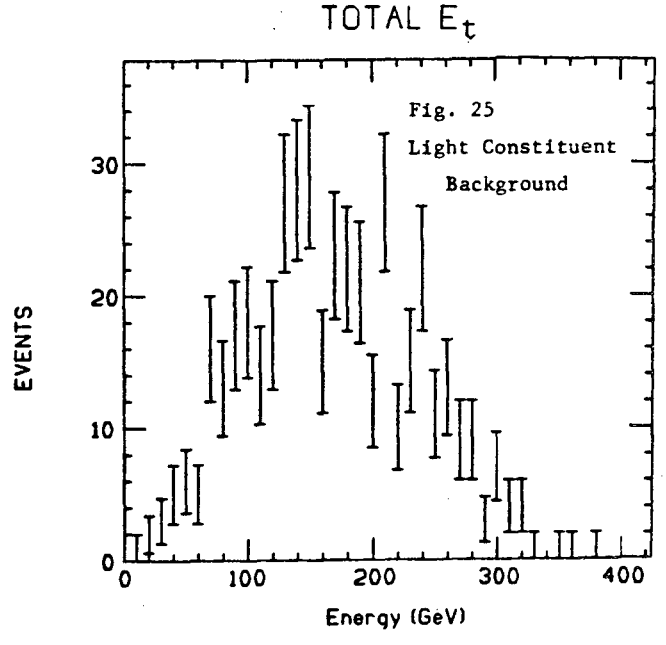

Fig. 24b Event characteristics of gluino pair production simulated through the D1 detector with $m_{\tilde{g}}$ = 1 TeV. We have assumed $\tilde{g} \to qq\tilde{\gamma}$, with $m_{\tilde{\gamma}} = 0$.

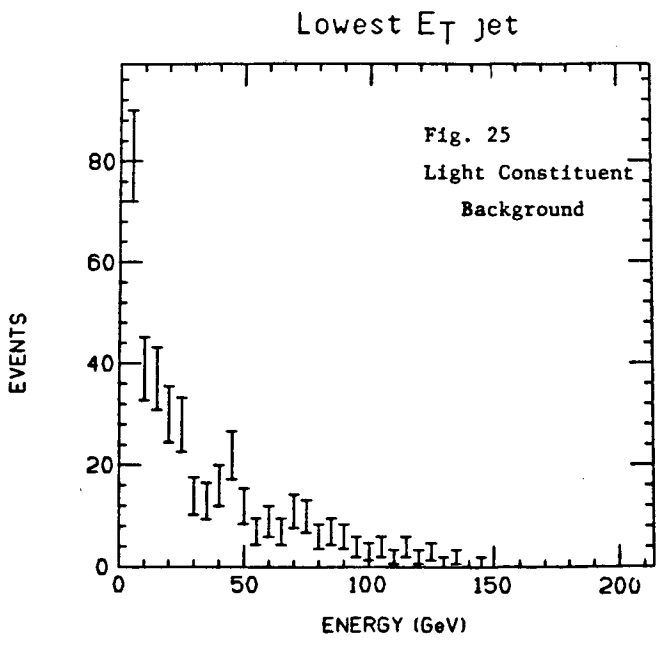

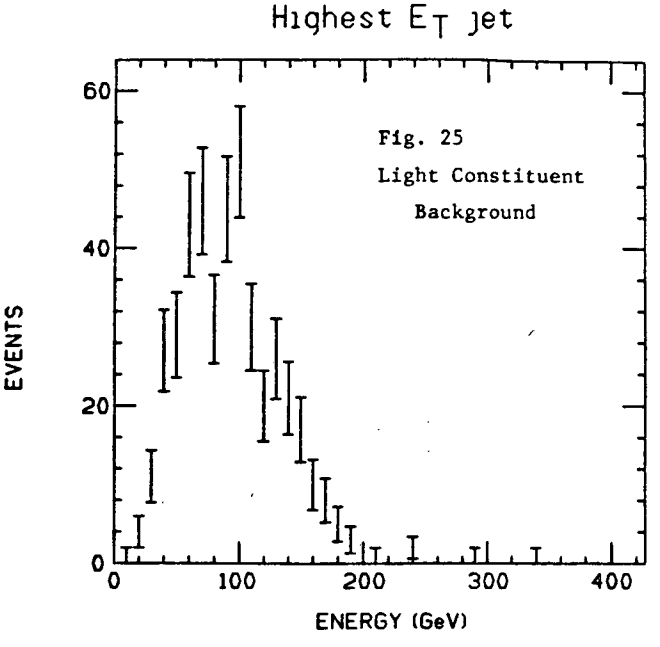

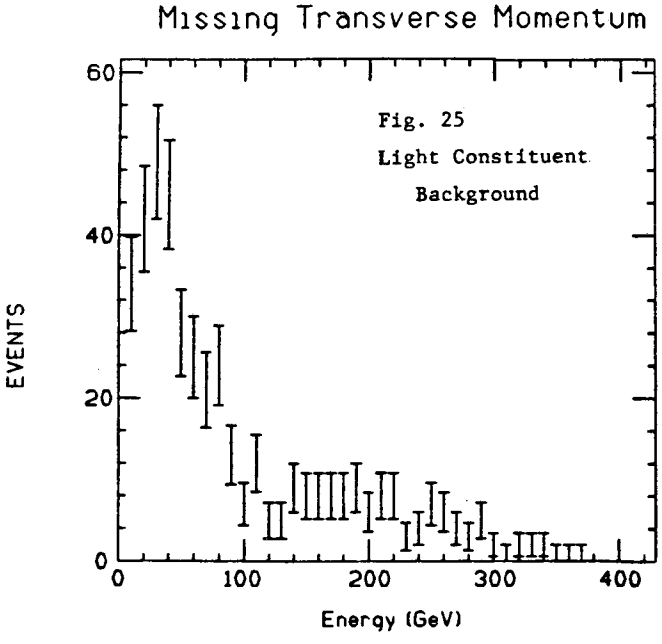

Fig. 25 General characteristics of light-constituent background simulated through the D1 detector.

Fig. 26

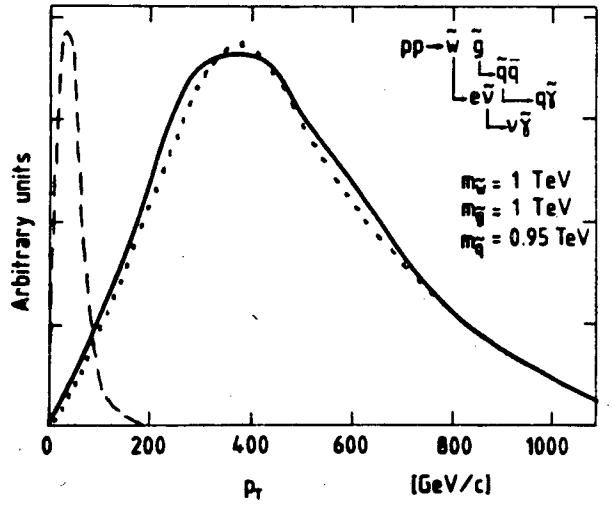

Fig. 26 $pp \to \tilde{W}\tilde{g} + X$ as given by a refined generator. The solid line is the E_T of the electron, the dotted line is the E_T of the highest jet and the dashed line is the E_T of the lowest E_T jet. We have taken $m_{\tilde{\nu}} = m_{\tilde{\gamma}} = 0$. Figs. 26 and 27 also appear in Ref. 14.

Fig. 27a

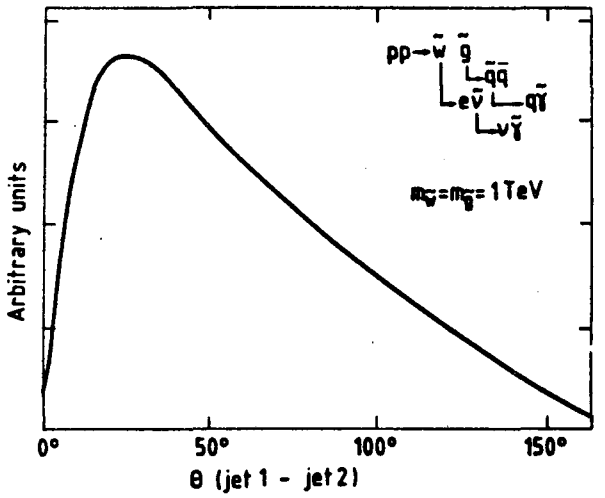

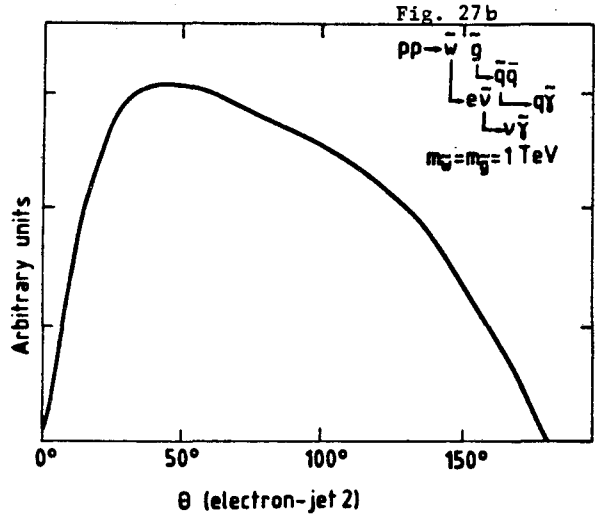

Fig. 27 $pp \to \tilde{W}\tilde{g} + X$ as given by a refined generator: a) Difference in spatial angle between the two q jets coming from $\tilde{g}$ decay; b) Difference in spatial angle between the highest E_T jet and the electron. We have assumed $m_{\tilde{\gamma}} = m_{\nu} = 0$.

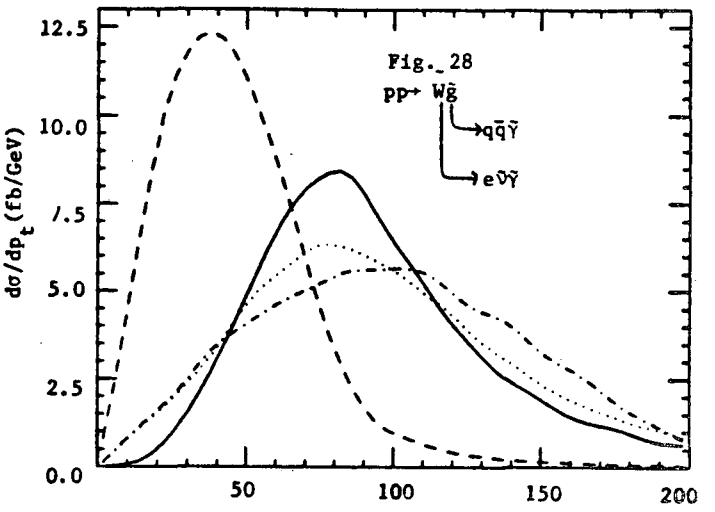

Fig. 28 The distribution of transverse momentum for $pp \to W\tilde{g} + X$ with $m_{\tilde{W}} = m_{\tilde{g}} = 200$ GeV, $m_{\tilde{q}} = 100$ GeV and $m_{\tilde{\gamma}} = 0$. The solid line is the highest E_T jet, the dashed line the lowest E_T jet, and the dash-dotted line the electron.

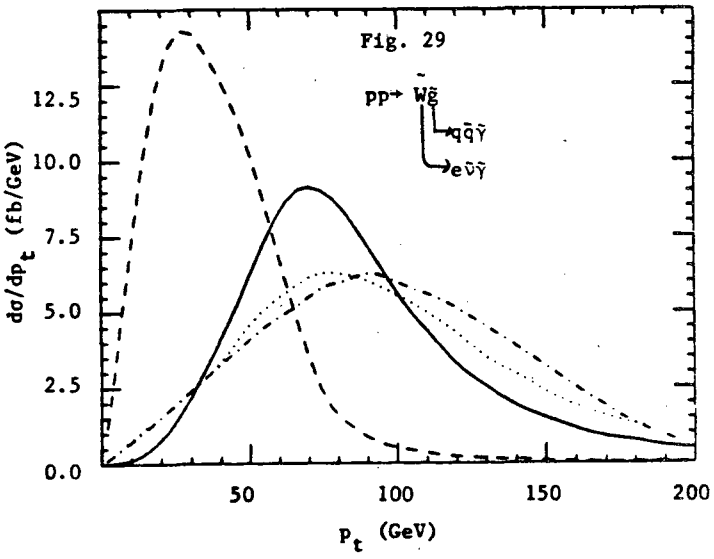

Fig. 29 Same as Fig. 28, but with $m_{\tilde{\gamma}} = 50$ GeV.

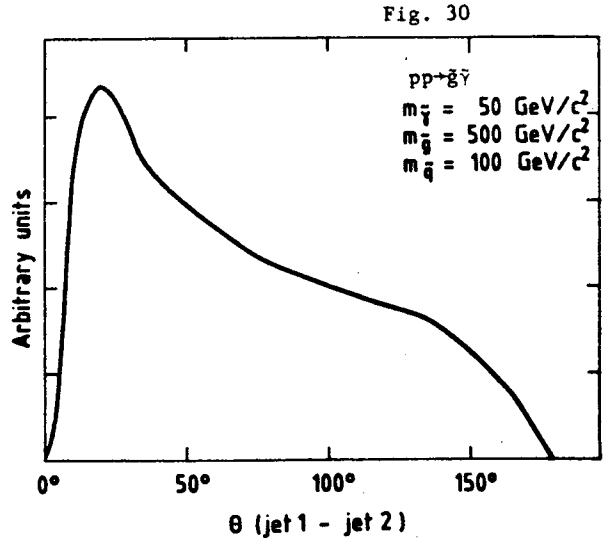

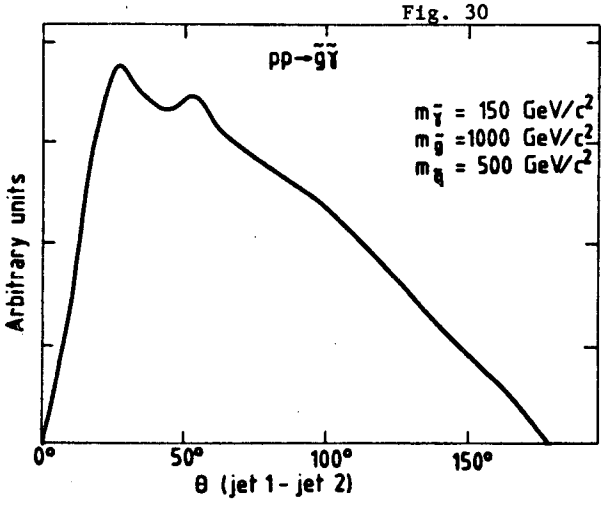

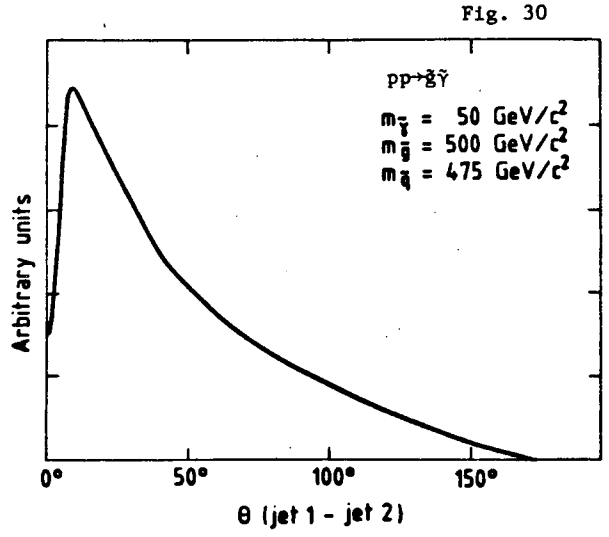

Fig. 30 $pp \rightarrow \tilde{g}\tilde{\gamma} + X$ as given by a refined generator: Difference in spatial angle between the two-q jets produced in $\tilde{g}$ decay, for different mass of sparticles (assuming $\tilde{\gamma}$ is massive).

TECHNICAL INFORMATION DEPARTMENT
LAWRENCE BERKELEY LABORATORY
UNIVERSITY OF CALIFORNIA
BERKELEY, CALIFORNIA 94720